Cell Reports
Article

Dual Engagement of the NLRP3 and AIM2 Inflammasomes by *Plasmodium*-Derived Hemozoin and DNA during Malaria

Parisa Kalantari,[1] Rosane B. DeOliveira,[1,5] Jennie Chan,[1,5] Yolanda Corbett,[2] Vijay Rathinam,[1] Andrea Stutz,[3] Eicke Latz,[1,3] Ricardo T. Gazzinelli,[1,4] Douglas T. Golenbock,[1,6] and Katherine A. Fitzgerald[1,6,*]

[1]Division of Infectious Diseases and Immunology, University of Massachusetts Medical School, Worcester, MA 01605, USA
[2]Dipartimento di Scienze Farmacologiche e Biomolecolari, Università Degli Studi di Milano, Via Pascal 36, Milano 20133, Italy
[3]Institute of Innate Immunity, Biomedical Center, 1G008, University Hospitals, University of Bonn, Sigmund-Freud-Strasse 25, Bonn 53127, Germany
[4]Department of Parasitology and Department of Biochemistry and Immunology, Biological Sciences Institute, Federal University of Minas Gerais, Avenida Antonio Carlos 6627, Belo Horizonte, MG 31270, Brazil
[5]These authors contributed equally to this work
[6]These authors contributed equally to this work
*Correspondence: kate.fitzgerald@umassmed.edu
http://dx.doi.org/10.1016/j.celrep.2013.12.014

SUMMARY

Hemozoin (Hz) is the crystalline detoxification product of hemoglobin in *Plasmodium*-infected erythrocytes. We previously proposed that Hz can carry plasmodial DNA into a subcellular compartment that is accessible to Toll-like receptor 9 (TLR9), inducing an inflammatory signal. Hz also activates the NLRP3 inflammasome in primed cells. We found that Hz appears to colocalize with DNA in infected erythrocytes, even before RBC rupture or phagolysosomal digestion. Using synthetic Hz coated in vitro with plasmodial genomic DNA (gDNA) or CpG oligodeoxynucleotides, we observed that DNA-complexed Hz induced TLR9 translocation, providing a priming and an activation signal for inflammasomes. After phagocytosis, Hz and DNA dissociate. Hz subsequently induces phagolysosomal destabilization, allowing phagolysosomal contents access to the cytosol, where DNA receptors become activated. Similar observations were made with *Plasmodium*-infected RBCs. Finally, infected erythrocytes activated both the NLRP3 and AIM2 inflammasomes. These observations suggest that Hz and DNA work together to induce systemic inflammation during malaria.

INTRODUCTION

Malaria continues to be one of the most devastating global health problems in human history. The overwhelming majority of cases of life-threatening malaria are caused by infection with *Plasmodium falciparum* (*Pf*), mostly in children under 5 years of age (Snow et al., 2005). *Plasmodium spp.* replicate inside red blood cells (RBCs). The rupture of parasitized RBCs induces a proinflammatory cytokine storm that coincides with fever in malaria patients (Grau et al., 1989; Kwiatkowski and Nowak, 1991). Excessive production of several cytokines, including tumor necrosis factor alpha (TNFα) (Grau et al., 1989; Kwiatkowski et al., 1990), interferon gamma (IFNγ) (Grau et al., 1989), interleukin-12 (IL-12) (Grau et al., 1989), and IL-1β (Franklin et al., 2009), have all been linked to disease. IL-1β is a highly synergistic cytokine and its regulation has the potential to radically modify the expression and effects of other immunomodulators (Last-Barney et al., 1988; Stashenko et al., 1987).

Several components of the *Plasmodium* parasite have been proposed to act as ligands for host receptors (Gazzinelli and Denkers, 2006). Parasite DNA represents a major trigger of innate immunity during infection. The genome of *Plasmodium* contains highly stimulatory CpG motifs, which activate TLR9 (Gowda et al., 2011; Parroche et al., 2007; Pichyangkul et al., 2004). The genome of *Plasmodium* is also highly AT rich (Gardner et al., 2002). An AT-rich stem-loop motif that is present in abundance in both *P. falciparum* and *P. vivax* has been shown to engage a cytosolic DNA-sensing pathway involving STING, TBK1, and IRF3 (Sharma et al., 2011). As a result of the proteolysis of hemoglobin in the digestive vacuole of the parasite, toxic heme accumulates. Plasmodial species have the capability to polymerize heme into the inert crystal Hz inside their food vacuole. This crystal is released from infected erythrocytes during schizogony. Once liberated, Hz is rapidly phagocytosed by immune cells, where it activates Src kinases (Shio et al., 2009) and induces the production of proinflammatory cytokines (Barrera et al., 2011; Jaramillo

et al., 2005; Pichyangkul et al., 1994; Sherry et al., 1995). Hz is often "synthesized" in the laboratory from hemin. In contrast to synthetic Hz (sHz), natural Hz (nHz) prepared from *Pf* cultures is bound by proteins and plasmodial DNA (Parroche et al., 2007). The immunological activity of pure Hz (i.e., sHz that has no hemin-associated contaminants) is controversial.

Hz has been proposed to be a ligand for TLR9 (Coban et al., 2005). Our group found that the TLR9-stimulatory capacity of nHz was dependent on *Plasmodium* DNA on the surface of the crystal, and not the Hz itself (Parroche et al., 2007). Although the transcriptional activity induced by Hz requires the presence of surface DNA, Hz itself does have immunological activity. sHz activates the Nod-like Receptor containing Pyrin domain 3 (NLRP3) inflammasome, resulting in the production of IL-1β and IL-18 (Dostert et al., 2009; Griffith et al., 2009; Reimer et al., 2010; Shio et al., 2009).

IL-1β-mediated fever is one of the hallmarks of malaria (Brown et al., 1999; Clark et al., 1994; Clark and Rockett, 1994) and the inflammasome is central to its regulation. The inflammasome is a multiprotein complex that is responsible for the processing and secretion of IL-1β. Mature IL-1β production requires priming signals to induce transcription of pro-IL-1β and NLRP3, and a second signal to initiate inflammasome assembly and activation.

The NLRP3 inflammasome senses a wide range of signals (Mariathasan et al., 2004), including crystalline materials such as monosodium urate and cholesterol crystals (Duewell et al., 2010; Martinon et al., 2006). These particulates trigger lysosomal deterioration and the release into the cytosol of lysosomal contents, which then activate NLRP3 (Duewell et al., 2010; Halle et al., 2008; Hornung et al., 2008). Absent in melanoma 2 (AIM2), a member of the (HIN)-200 family, recognizes cytosolic double-stranded DNA (Bürckstümmer et al., 2009; Hornung et al., 2009; Rathinam et al., 2010).

Here, we report our findings on the molecular basis for IL-1β production in malaria. Our data suggest that DNA drives many aspects of the innate immune response during malaria, and that it gets into the phagocytic compartment of cells either through the ingestion of free Hz, which can traffic associated DNA, or the phagocytosis of Hz-laden infected RBCs, where it activates TLR9. The full activity of plasmodial DNA depends on the parallel activities of Hz. We suggest that the parasite components Hz and DNA play a synergistic role in inflammation and tissue damage during disease.

RESULTS

DNA-Coated Hz Provides All of the Signals Necessary for NLRP3 Inflammasome Activation and Production of Mature Cytokines

Our group previously reported that TLR9 binds to Hz through its interaction with parasite DNA present on the surface of Hz (Parroche et al., 2007). However, it was not clear whether the DNA found on the surface of nHz bound to the surface of the crystal before or after erythrocyte rupture. Hz is synthesized inside the food vacuole of the parasite, which is completely separate from its nucleus. During the process of parasite expansion, there is constant turnover of a subpopulation of parasites. We hypothesized that during this process of parasite turnover, Hz may be exposed to parasite DNA. In order to address this issue, we injected *P. berghei* ANKA-infected mice (day 9 of infection) with bromodeoxyuridine (BrdU), a thymidine analog that incorporates into newly synthesized DNA. After three injections, the mice were bled. The blood was enriched to achieve a preparation of RBCs that were ~90% infected, stained with a fluorescein isothiocyanate (FITC)-conjugated antibody to BrdU, and examined by reflection confocal microscopy, a technique that takes advantage of the birefringence of the Hz crystal (and which we used throughout this study). Approximately 19% of the intraerythrocytic Hz crystals that were observed by confocal microscopy appeared to colocalize with BrdU (Figure 1A, middle), and 81% did not (Figure 1A, bottom). In addition, we found that BrdU does not interact nonspecifically with nHZ (Figure S1A). Rather, the data suggest that BrdU was incorporated into the parasite genome, and the DNA later became associated with nHz during the natural process of parasite growth and turnover, probably due to blood-derived innate immune defenses. We note that interpretation of these studies is limited by the nature of reflection confocal microscopy, which precludes imaging in the Z dimension.

We previously suggested that Hz enables CpG motifs in plasmodial DNA to activate TLR9 within the phagolysosome (Parroche et al., 2007). These initial studies suggested that nHz triggered TLR9 translocation. In order to test this idea, we made sHz/DNA complexes and then assessed the fate of the DNA and sHz by reflection confocal microscopy. Scanning electron micrographs of our sHz crystals show that they are homogeneous in size and shape (Figure S1B). sHz failed to induce proinflammatory cytokines such as TNFα (Figure S1C), consistent with data from other groups (Dostert et al., 2009; Griffith et al., 2009; Parroche et al., 2007; Reimer et al., 2010).

We found that Hz-laden CpG DNA (sHz/CpG) was rapidly internalized into the phagolysosome of bone-marrow-derived macrophages (BMDMs) along with its Alexa647-labeled DNA cargo (Figure 1B, top). Although free CpG DNA engages TLR9 in the early endosomal compartment, Rab 4 (an early endosomal marker) did not colocalize with sHz (Figure 1B, bottom). In order to determine whether this is relevant to what occurs in vivo, we incubated BMDMs with *P. berghei*-infected RBCs (iRBCs) from mice that were injected with BrdU. As shown in Figure 1C, by 1 hr, iRBCs were engulfed by the phagolysosome, where nHz was observed together with fluorescently labeled plasmodial DNA (Figure 1D, middle). However, by the 12 hr time point, Hz and DNA dissociated (Figure 1D, bottom) and no longer appeared to be within the phagosome.

The activity of the inflammasome is commonly broken down into a "priming" step and a second step that results in the assembly of a larger complex that generates mature cytokines. We used a macrophage cell line that expresses ectopic ASC-CFP to examine the kinetics of inflammasome activation by Hz (Bauernfeind et al., 2009). Inflammasome assembly was visualized in ~40% of the macrophages that were exposed to sHz/CpG within 6 hr of incubation (Figures 1E and S1D). In addition,

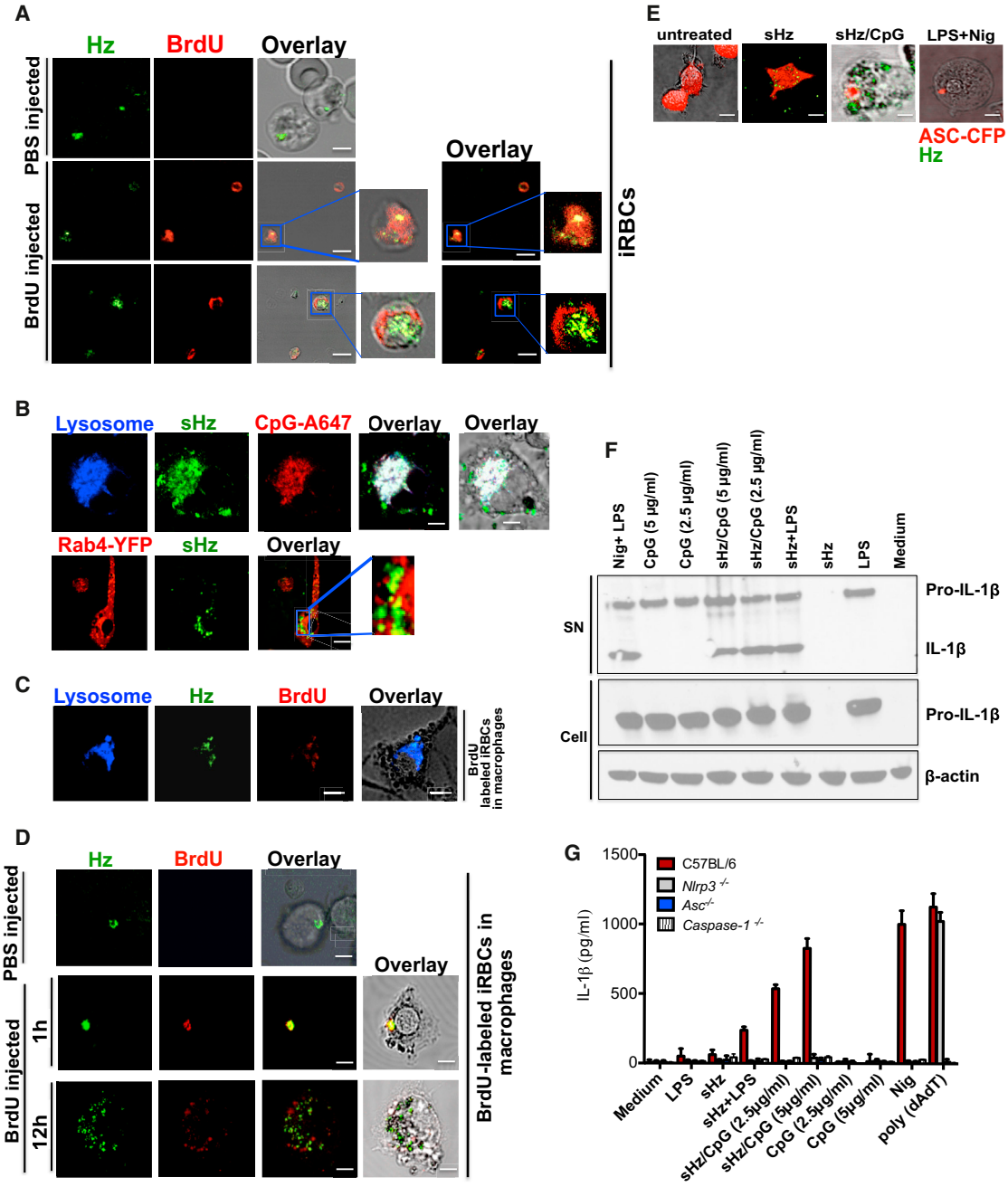

Figure 1. Hz Colocalizes with DNA In Vivo and Is Internalized into the Phagolysosome, Where It Has the Capacity to Prime Macrophages and Activate the NLRP3 Inflammasome

(A) Erythrocytes from PBS-injected and BrdU-injected *P. berghei* ANKA-infected mice were stained with FITC-conjugated BrdU antibody and subjected to confocal microscopy. Boxed areas in middle and bottom panels are enlarged (3×). Scale bars, 3 μm (top panel), 7.8 μm (middle panel), and 7.8 μm (bottom panel).

(B) Top: sHz (100 μg/ml) was incubated with CpG-Alexa 647 (5 μg/ml) for 2 hr. The complex was washed three times with PBS before incubation with immortalized BMDMs, and imaged by confocal microscopy after 30 min. Scale bar, 5 μm. Bottom: Confocal microscopy of immortalized BMDMs stably transduced with Rab4-YFP and stimulated with sHz crystals (100 μg/ml) for 2 hr. Scale bar, 15 μm. The boxed areas are enlarged on the right, demonstrating lack of colocalization.

(C) RBCs from BrdU-injected *P. berghei* ANKA-infected mice were stained and prepared as in (A). BMDMs were incubated with iRBCs (multiplicity of infection [moi]: 5–1) × 1 hr and stained with LysoTracker. Scale bar, 5 μm.

(D) RBCs from PBS- or BrdU-injected *P. berghei* ANKA-infected mice were incubated with BMDMs (moi: 5–1), stained with FITC-conjugated BrdU antibody, and subjected to confocal microscopy after 1 or 12 hr. Scale bars, 20 μm (top panel) and 20 μm (bottom panel).

(legend continued on next page)

sHz/CpG provided all of the necessary signals to result in the production of mature IL-1β (Figures 1F and S1E), in contrast to sHz or CpG DNA alone. In order to determine which inflammasome was being activated, we analyzed cell lines derived from several knockout mice. This experiment (Figure 1G) confirmed the observations of several other groups that the second signal in NLRP3 inflammasome activation could be provided by sHz (Dostert et al., 2009; Griffith et al., 2009; Reimer et al., 2010; Shio et al., 2009). These results were confirmed in primary wild-type (WT) and *Nlrp3*-deficient macrophages (Figure S1F). Although these experiments were performed using the mouse CpG oligodeoxynucleotide (ODN) known as 1826, we observed similar results with CpG ODNs derived from the genome of *Pf* (Figure S1G). In contrast to NLRP3, NLRP6 (Elinav et al., 2011) and NLRP12 (Arthur et al., 2010) were dispensable for sHz/CpG-mediated IL-1β release (Figure S1H).

Hz Traffics *Pf* Genomic DNA into the Lysosomal Compartment, Resulting in Accessibility to TLR9

Confocal imaging of sHz/CpG within macrophages revealed that over time, DNA bound to Hz dissociated from the crystal (Figures 1D, bottom, and 2A) and that Hz mediated a loss of phagolysosomal integrity. Surprisingly, as the phagolysosome disintegrated, the crystal appears to have been released, whereas the CpG DNA remained bound to the lysosomal compartment, as defined by staining with LysoTracker (Figure 2B). Since LysoTracker selectively stains all acidic compartments, we also used lamp1-Kate2 macrophages (which express fluorescent lamp1) and obtained similar results (Figures 5F and S2A). We hypothesized that CpG DNA remained with the phagolysosome because it was bound to endosomal TLRs, such as TLR3, TLR7, and TLR9. When the same experiment was performed with macrophages from Unc93b mutant mice, which fail to translocate TLR3, TLR7, and TLR9 to the lysosomal compartment (Tabeta et al., 2006), DNA dissociated from the sHz and transited to the cytosol (Figure 2C).

We previously hypothesized that Hz traffics DNA into a lysosomal compartment where it could engage TLR9 (Parroche et al., 2007). Here, we used BMDMs from a transgenic mouse that expresses GFP-tagged TLR9 (Figure 2D) to directly test our hypothesis. When exposed to sHz, TLR9 remained in the endoplasmic reticulum. When fluorescently labeled free CpG ODNs were internalized into the endolysosomal compartment, TLR9 almost completely colocalized with the ODN within 30 min, as expected (Latz et al., 2004). Similarly, sHz/CpG was internalized rapidly into phagosomes, and provided the necessary signals for TLR9 translocation. sHz that was coated with *Pf* genomic DNA (gDNA) resulted in movement of TLR9 to the phagolysosome, similar to what was observed for sHz/CpG (Figure 2D).

The translocation of TLR9 to the phagosome plays a critical role in priming the NLRP3 inflammasome. Although sHz/CpG and sHz/*Pf* gDNA were sufficient to induce the production and secretion of active IL-1β, this did not occur in macrophages from *Tlr9*$^{-/-}$ mice (Figure 2E). Indeed, a true physiologic role for TLR9 in IL-1β production is suggested by the finding that sHz/*Pf* gDNA and sHz/CpG were nearly identical in dependence on TLR9 expression in order to induce the secretion of IL-1β (Figure 2E).

Although sHz interacts weakly with *Pf* gDNA (Jaramillo et al., 2009), it has been shown that host and plasmodial proteins interact with the Hz crystal (Ashong et al., 1989; Goldie et al., 1990; Jaramillo et al., 2009). Accordingly, we coated sHz with fetal bovine serum (FBS) and then incubated the protein-coated sHz with *Pf* gDNA. In contrast to "naked" sHz, serum-coated sHz interacted strongly with *Pf* gDNA (Figure S2B). These findings imply that proteins bind to nHz and form a bridge with *Pf* gDNA during infection. Indeed, several years ago, we found that proteinase K treated nHz lost its DNA coating (data not shown). Taken together, these findings may explain an observation made almost 20 years ago by Pichyangkul et al. (1994), who reported that protease-treated nHz lost its ability to induce TNFα and IL-1β from human monocytes. Protease treatment undoubtedly removed the surface DNA from nHz that was responsible for cytokine induction.

NLRP3 Activation by Hz Requires Phagocytosis of the Crystals and Leads to Phagolysosomal Destabilization

As can be seen in Figure 3A, the inhibition of crystal engulfment by cytochalasin D resulted in dose-dependent disruption of NLRP3 activity, as evidenced by the inhibition of IL-1β production in macrophages exposed to sHz-complexed with CpG DNA (Figure 3B). Cytochalasin D had no effect on the release of IL-1β upon stimulation with the potassium ionophore nigericin (Figure 3B).

Similarly to sHz, macrophages actively engulf nHz crystals. Within a few hours of phagocytosis, nHz induced phagolysosomal instability. For example, in Figure 3C, one can see that untreated macrophages accumulate fluorescent dextran in lysosomes and form a punctate staining pattern. In contrast, macrophages that have engulfed nHz no longer accumulate fluorescent dextran in their lysosomal compartment due to the loss of phagolysosomal integrity. These experiments were repeated with sHz, with similar results (Figure S3A). To further evaluate the effect of Hz on the shape and size of lysosomes, we stained macrophages with acridine orange. This dye binds to both DNA

(E) BMDMs stably expressing ASC-CFP were treated with sHz/CpG (5 μg/ml), sHz only (100 μg/ml), or LPS (100 ng/ml) × 2 hr and then treated with nigericin (10 μM), a K+ ionophore that activates NRLP3. The formation of ASC pyroptosomes was visualized by confocal microscopy. Fields are representative of at least ten fields of view and three independent experiments. Scale bars from left to right, 15 μm, 10 μm, 5 μm, and 5 μm. sHz (green) was visualized by reflection microscopy.

(F) Immunoblot analysis of IL-1β cleavage to mature IL-1β (p17) in supernatants (SN) and cell extracts (Cell) from WT murine BMDMs stimulated as described in (G).

(G) ELISA of released IL-1β by immortalized BMDMs from WT, *Nlrp3*$^{-/-}$, *Asc*$^{-/-}$ and *casp1*$^{-/-}$ macrophages that were unprimed or primed or with LPS (100 ng/ml) for 2 hr, and then left unstimulated or stimulated for an additional 12 hr with sHz, sHz/CpG (sHz: 100 μg/ml; CpG: 2.5 μg/ml and 5 μg/ml), or CpG (2.5 μg/ml and 5 μg/ml), or transfected with 1.5 μg/ml poly (dAdT). Nigericin (Nig) was used as a control. Poly (dAdT) was used as an AIM2 inflammasome-activating control. Data are presented as mean ± SD of triplicates and are representative of three independent experiments.

See also Figure S1.

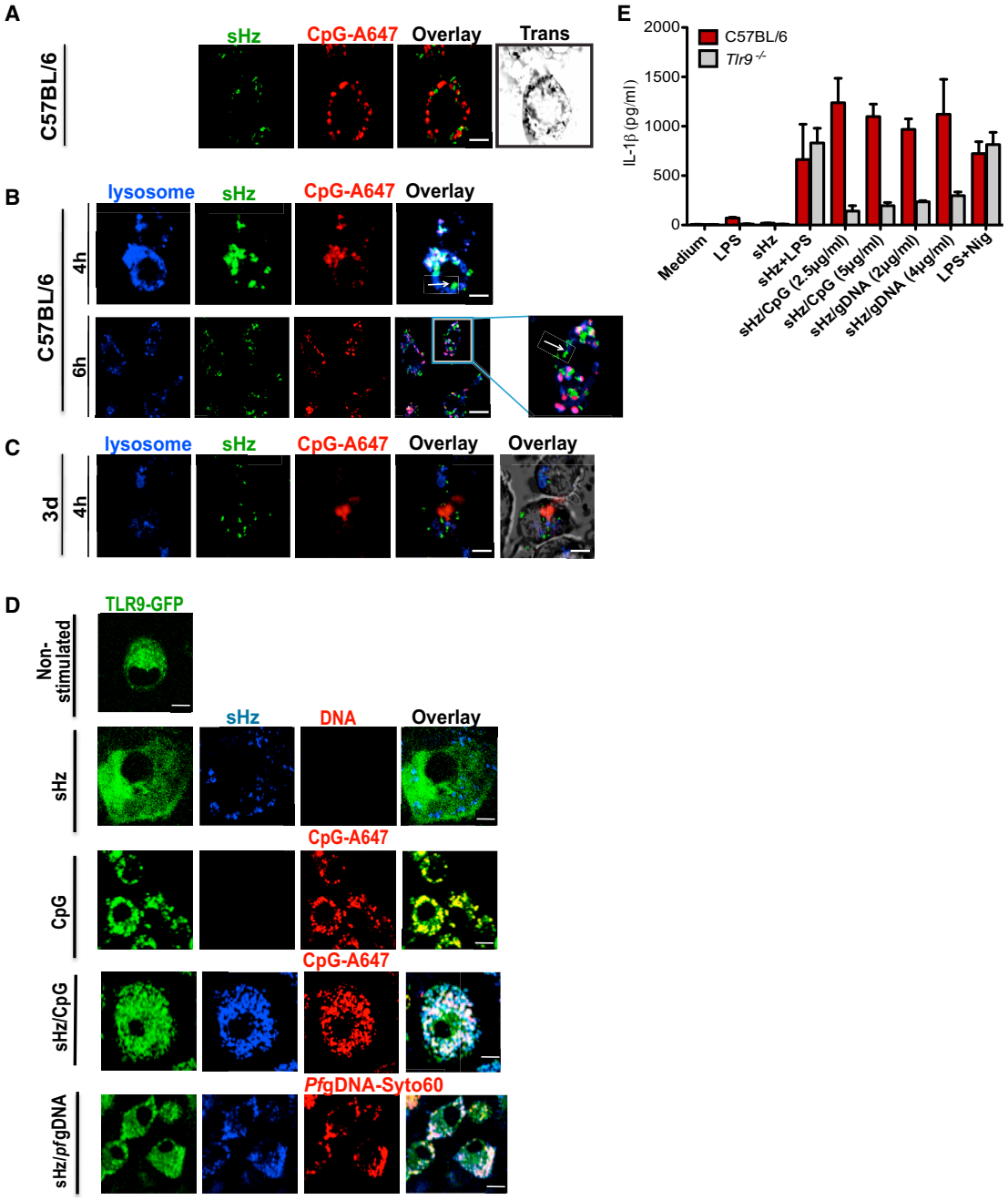

Figure 2. sHz/CpG or sHz/*Pf* gDNA Induces TLR9 Translocation to the Phagosome, followed by TLR9-Dependent Release of IL-1β

(A) sHz/CpG-A 647 (5 μg/ml) was added to the cells and subjected to confocal microscopy after 6 hr of incubation. Scale bar, 5 μm.

(B) BMDMs were incubated with sHz/CpG-A 647 (5 μg/ml) × 4 hr or 6 hr and stained with LysoTracker (blue). Scale bars, 10 μm (top panel) and 5 μm (bottom panel). Boxed area in main image at right is enlarged (2.5×). The arrow (in both top and bottom panels) indicates Hz in the cytosol.

(C) "3d" macrophages functionally deficient in TLR3, TLR7, and TLR9 were incubated with CpG-A647 DNA × 4 hr. Scale bar, 10 μm. Fields are representative of at least ten fields of view and three independent experiments.

(D) Immortalized BMDMs isolated from transgenic TLR9-GFP mice were left untreated or incubated with sHz (100 μg/ml), CpG-Alexa 647 (5 μg/ml), sHz/CpG-Alexa 647 (5 μg/ml), and sHz/*Pf* gDNA-Syto60 (4 μg/ml) for 30 min and living cells were visualized by confocal microscopy. Fields are representative of at least ten fields of view and three independent experiments. Scale bars from top to bottom, 5 μm, 15 μm, 5 μm, 15 μm, and 5 μm.

(E) ELISA of IL-1β production by WT and *Tlr9*$^{-/-}$ BMDMs, primed or unprimed for 2 hr with LPS (100 ng/ml) and then left unstimulated or stimulated with the indicated amounts of sHz, sHz/CpG complex, sHz/*Pf* gDNA, or nigericin (10 μM). Supernatants were analyzed for IL-1β 12 hr after stimulation. Data are presented as mean ± SD of triplicates and are representative of three independent experiments.

See also Figure S2.

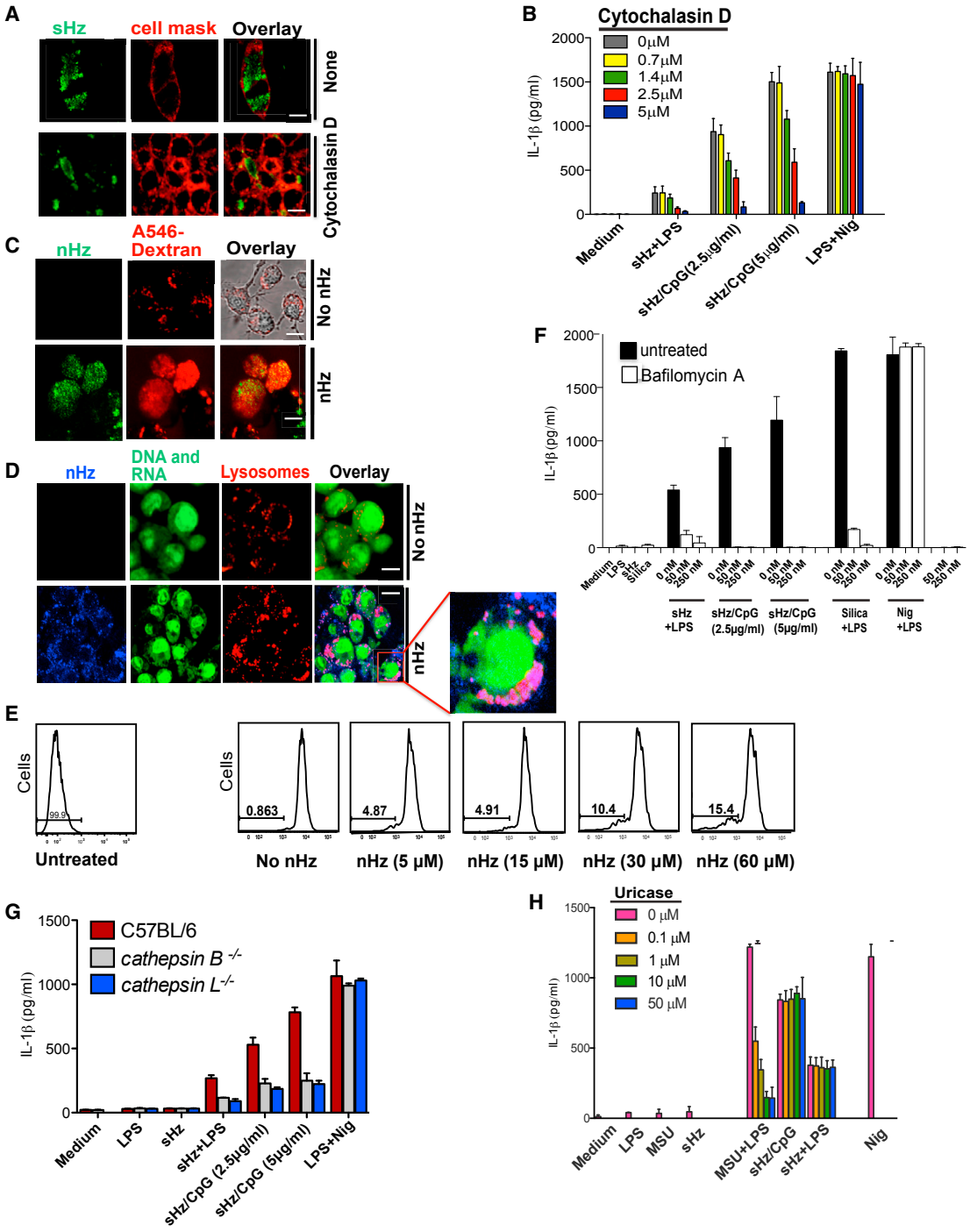

Figure 3. Phagocytosis of Crystals Leads to Phagolysosomal Destabilization and Is Necessary for IL-1β Release

(A) Confocal microscopy of BMDMs stimulated with sHz (100 μg/ml) for 2 hr in the absence and presence of cytochalasin D (2.5 μM). Cell membranes were stained with cell mask (red). Scale bars, 5 μm (top) and 20 μm (bottom).

(B) ELISA of the release of IL-1β into supernatants of immortalized BMDMs left untreated or treated with increasing concentrations of cytochalasin D and then stimulated for 12 hr with sHz or sHz/CpG complex.

(C) Confocal microscopy of immortalized BMDMs incubated with A546-Dextran (10 kDa) for 45 min and then either left untreated or stimulated with 100 μM nHz for 4 hr. Scale bar (top and bottom panels), 10 μm.

(D) Macrophages were stained with acridine orange (0.05 mg/ml) for 10 min and then stimulated with nHz (100 μM); 4 hr after stimulation, cells were analyzed by confocal microscopy. Fields are representative of at least ten fields of view and three independent experiments. Scale bars, 10 μm (top) and 20 μm (bottom). Boxed area is enlarged (9×).

(legend continued on next page)

and RNA in the nucleus and cytosol, where it fluoresces green (525 nm). As shown in Figure 3D, acridine orange becomes highly concentrated in the lysosomal compartment under acidic conditions and fluoresces red (600–650 nm) (Hornung et al., 2008). The loss of phagolysosomal integrity was quantified by flow cytometry, which showed a dose-dependent loss of red fluorescence as acridine orange escaped to the cytosol (Figure 3E). Note that the experiments shown in Figures 3D and 3E were also repeated with sHz, with similar results (data not shown). Taken together, these results indicate that phagocytosis of Hz crystals leads to the loss of phagolysosomal integrity, resulting in leakage of the lysosomal contents into the cytosol.

We next tested the effects of bafilomycin A, an H^+ ATPase inhibitor that leads to the neutralization of lysosomal pH and prevents the activation of most lysosomal proteases, including cathepsins. Bafilomycin A significantly blocked the sHz/CpG-mediated release of IL-1β, but had no effect on nigericin (Figure 3F). These data suggest that lysosomal acidification is critical in sHz/CpG-mediated inflammasome activation. When bafilomycin A was added to cells before their exposure to sHz, the phagolysosome did not remain intact, suggesting that phagolysosomal integrity is independent of lysosomal pH (data not shown). Several cathepsins, including cathepsins B and L, have been reported to be important in mediating inflammasome activation in response to crystal exposure (Duewell et al., 2010; Hornung et al., 2008). Immortalized BMDMs from *Ctsb*$^{-/-}$ and *Ctsl*$^{-/-}$ mice had reduced levels of IL-1β after sHz/CpG exposure (Figure 3G). Similarly, specific inhibitors of various cathepsins inhibited IL-1β release (Figure S3B). These data suggest that the cathepsins might play a role in Hz-mediated inflammasome activation.

A number of studies have demonstrated a role for uric acid in the immune response to malaria (Guermonprez et al., 2013; Lopera-Mesa et al., 2012; Orengo et al., 2008, 2009; van de Hoef et al., 2013), and released urate has been suggested as the cause of Hz-induced inflammasome activation in vivo (Griffith et al., 2009). To determine whether sHz activates NLRP3 via the release of uric acid, we pretreated macrophages with uricase before adding sHz/CpG. Uricase added to monosodium urate-stimulated cells resulted in a dose-dependent decrease in IL-1β release, but had no effect on the response to sHz/CpG-treated cells (Figure 3H). Hence, sHz did not appear to be activating NLRP3 through the release of uric acid.

Plasmodial gDNA on the Surface of Hz Induces Mature IL-1β Production in Macrophages through the AIM2 Inflammasome

Pf gDNA, when transfected into lipopolysaccharide (LPS)-primed macrophages, induced IL-1β release (Figure 4A). IL-1β production was independent of NLRP3 expression, but dependent on ASC and caspase-1, indicating that parasite gDNA is recognized by an alternative inflammasome (Figure 4A). AIM2 is a HIN-200 family member that directly binds cytosolic double-stranded DNA, resulting in the formation of inflammasomes. We transfected *Pf* gDNA into the cytosol of *Aim2*$^{+/+}$ and *Aim2*$^{-/-}$ primary macrophages, and discovered that AIM2 expression was essential for IL-1β production, regardless of the strain of *Pf* from which the gDNA was obtained (Figure 4B). The results of these functional assays were confirmed when cells were analyzed by confocal microscopy. ASC-CFP speck formation was activated by transfection of *Pf* gDNA; indeed, the gDNA colocalized with the developing ASC pyroptosome (Figures 4C and S4A), consistent with the prediction that the DNA binds directly to AIM2. In support of this hypothesis, we transfected *Pf* gDNA into macrophages that express AIM2-citrine. Speck formation was again observed, and AIM2 colocalized with the DNA (Figures 4D and S4B). Incubating these cells with sHz/*Pf* gDNA induced AIM2 pyroptosome formation (Figure S4C), whereas sHz alone (Figure 4D, bottom panel) did not induce AIM2 pyroptosome formation in AIM2-citrine cells. Conversely, transfection of *Pf* gDNA into cells that expressed fluorescently tagged NLRP3 (Bauernfeind et al., 2009) did not result in speck formation (Figure 4E). On the other hand, when *Pf* gDNA was introduced into unprimed cells on the surface of sHz via a phagocytic pathway, NLRP3 pyroptosome formation was observed (Figures 4E and S4D). These observations are consistent with the concept that when innate immune cells are exposed to sHz/DNA, the DNA can prime the macrophages via TLR9 in the phagosome, generating NLRP3 and pro-IL-1β. DNA subsequently directly activates the AIM2 inflammasome once it has access to the cytosol. The role of Hz, with respect to AIM2, is to allow DNA that enters cells via a phagocytic pathway access to the cytosol.

nHz Induces IL-1β Release through the Activation of Both NLRP3 and AIM2

During the *Plasmodium* life cycle, merozoites, digestive vacuoles containing Hz, as well as free Hz, are released into the blood stream upon schizont rupture. During this process, parasites and their products are rapidly internalized by phagocytes, especially those that reside in the liver and spleen. In turn, these cells produce cytokines, chemokines, and other immunomodulators. sHz complexed to CpG DNA triggers the inflammasome pathway, providing both an NF-κB signal to induce NLR and pro-IL-1β expression and a second signal to induce inflammasome assembly. We purified nHz from cultures of *Pf* and used that to stimulate cells in order to validate sHz/CpG as a model of nHz crystal.

(E) FACS analysis of immortalized BMDMs stained with acridine orange and treated with the indicated amounts of nHz × 4 hr. The numbers above the brackets indicate the percentage of macrophages that have lost acridine orange staining.
(F) ELISA of released IL-1β from unprimed or LPS-primed immortalized BMDMs pretreated with the indicated concentrations of bafilomycin A × 2 hr and then stimulated with sHz, sHz/CpG, or silica (500 μg/ml) × 12 hr.
(G) ELISA of released IL-1β by WT, *ctsb*$^{-/-}$, and *ctsl*$^{-/-}$ BMDMs left unstimulated or stimulated with sHz (100 μg/ml) or sHz/CpG for 12 hr.
(H) ELISA of IL-1β production by unprimed or LPS-primed immortalized murine BMDMs pretreated with indicated concentrations of uricase for 2 hr, stimulated with LPS (100 ng/ml) for another 2 hr, and then incubated with monosodium urate (500 μg/ml), sHz (100 μg/ml), and sHz/CpG (5 μg/ml) for 12 hr. Data are presented as mean ± SD of triplicates and are representative of three independent experiments.
See also Figure S3.

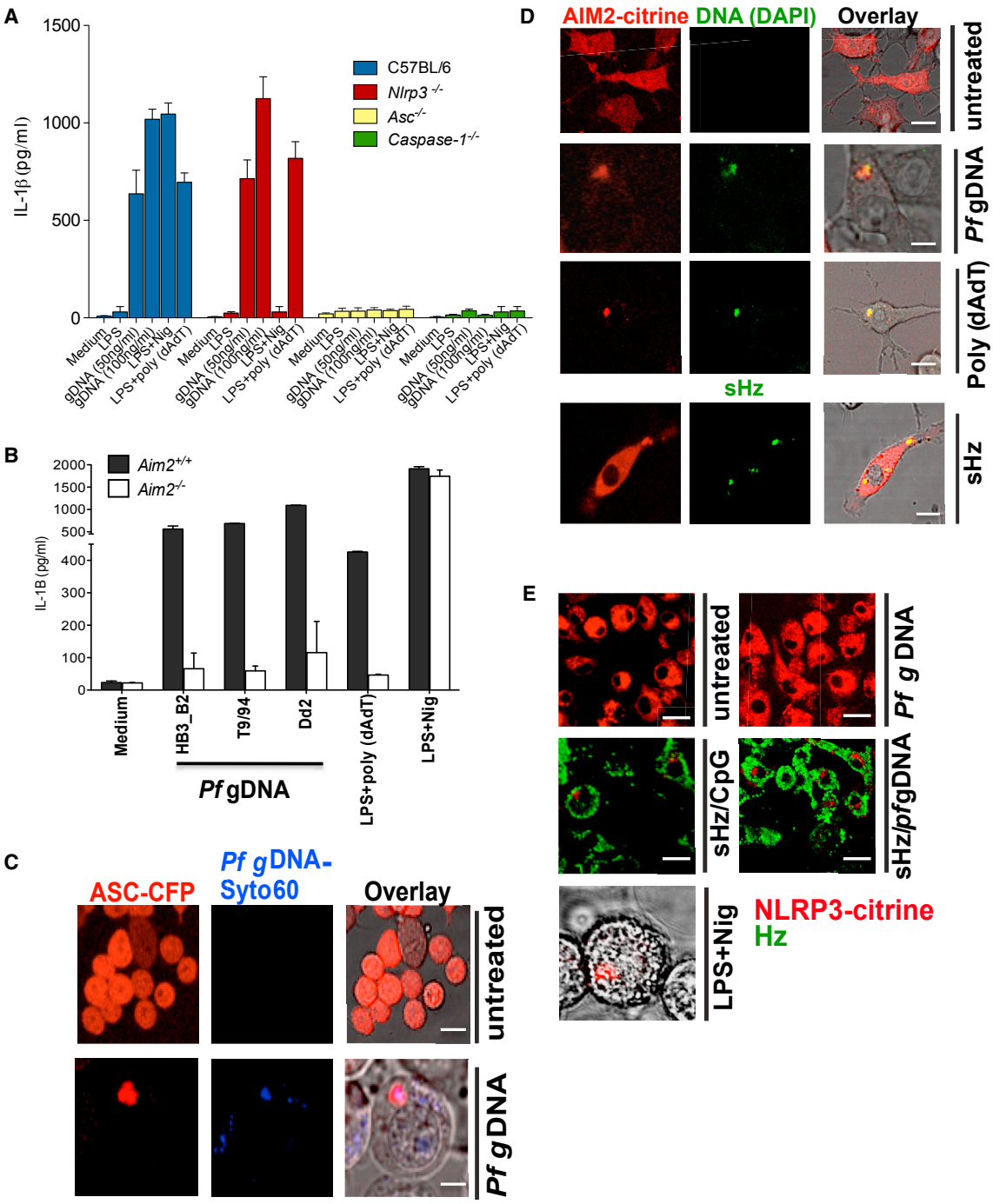

Figure 4. *Pf* gDNA Induces IL-1β through Activation of AIM2 Inflammasome

(A) We transfected 50 and 100 ng/ml of *Pf* gDNA (3D7) using Lipofectamine into LPS-primed (100 ng/ml × 2 hr), immortalized murine WT, *Nlrp3*$^{-/-}$, *Asc*$^{-/-}$, and *casp1*$^{-/-}$ BMDMs. After 12 hr, IL-1β was measured in the culture supernatants by ELISA.

(B) We transfected 100 ng/ml of gDNA from different strains of *Pf* (Dd2, T9/94, HB3-B2) using Lipofectamine into LPS-primed primary *Aim2*$^{+/+}$ and *Aim2*$^{-/-}$ BMDMs. Cell culture supernatants were used to measure IL-1β by ELISA. Data are presented as mean ± SD of triplicates and are representative of three independent experiments.

(C) Confocal microscopy of LPS-primed ASC-CFP cells left untransfected or transfected with 100 ng/ml Syto60-labeled *Pf* gDNA. Scale bars, 20 μm (top) and 5 μm (bottom).

(D) Confocal microscopy of LPS primed AIM2-citrine macrophages left untransfected or transfected with 100 ng/ml DAPI-labeled *Pf* gDNA or DAPI-labeled poly (dAdT) using Lipofectamine, or just incubated with sHz. Scale bar (from top to bottom), 15 μm, 5 μm, 15 μm, and 15 μm.

(legend continued on next page)

Examination of nHz by microscopy confirmed that it was free of contaminating iRBCs or parasites. As shown in Figures 5A and S5A, nHz caused the formation of ASC specks in immortalized BMDMs. In addition, nHz induced IL-1β release from primary C57Bl/6 macrophages (Figure 5B, top-left panel). This ability of nHz to induce IL-1β from BMDMs was dramatically diminished, but not abolished, when nHz was used to stimulate BMDMs from *Nlrp3*$^{-/-}$ mice (Figure 5B, top right). Similarly, BMDMs from *Aim2*$^{+/+}$ mice were highly responsive to nHz (Figure 5B, lower left), and responses were greatly diminished, but not abolished, in cells from *AIM2*$^{-/-}$ mice (Figure 5B, lower middle). When we crossed the *Aim2* knockout with the *Nlrp3* knockout mouse (*Aim2*$^{-/-}$*Nlrp3*$^{-/-}$), we found that the residual IL-1β-inducing activity was gone (Figure 5B, lower right).

In addition to the ability of nHz to induce IL-1β production, we evaluated cell viability using the vital probe calcein AM. nHz-induced inflammasome activation resulted in pyroptotic cell death in a dose-dependent manner in WT macrophages, but caused significantly less cell death in ASC- and caspase-1-deficient macrophages. *Nlrp3*-deficient macrophages were partly resistant to cell death (Figures S5B and S5C). We also incubated *Aim2*$^{+/+}$, *Aim2*$^{-/-}$, and *Nlrp3*$^{-/-}$*Aim2*$^{-/-}$ double-knockout BMDMs with nHz. nHz induced cell death in *Aim2*$^{+/+}$ BMDMs, but was rescued partly in *Aim2*$^{-/-}$ and almost completely rescued in *Nlrp3*$^{-/-}$*Aim2*$^{-/-}$ double-knockout BMDMs (Figure 5C), suggesting that NLRP3 and AIM2 inflammasomes together mediate most of the nHz-induced cell death in macrophages.

These observations were confirmed by western blots of livers harvested from animals injected with sHz/*Pf* gDNA. It should be noted that mammalian livers have a large quantity of preformed pro-IL-1β, presumably because the liver is constantly being primed by bacterial products absorbed from the gastrointestinal track. After injection with sHz/gDNA, the mature 17 kDa IL-1β was significantly reduced in the *Nlrp3*$^{-/-}$*Aim2*$^{-/-}$ double-knockout mice compared with littermate controls (Figure 5D and original blots in Figure S5D). Hence, sHz/*Pf* gDNA activates both the AIM2 and the NLRP3 inflammasomes.

Our in vitro results presented above revealed the potent capability of nHz to induce proinflammatory responses via NLRP3 and AIM2 inflammasomes. To confirm the physiological relevance of this finding in vivo, in the context of Hz-induced inflammation, we used a peritonitis model. Mice were injected intraperitoneally with sHz/*Pf* gDNA. The sHz/*Pf* gDNA induced a considerable increase in the recruitment of neutrophils to the peritoneal cavity in WT mice, but not in *Nlrp3*$^{-/-}$, *Aim2*$^{-/-}$, or *Nlrp3*$^{-/-}$*Aim2*$^{-/-}$ double-knockout mice (Figure 5E).

Overall, the data suggest that the initial signals necessary for the synthesis of pro-IL-1β arise from DNA activation of TLR9. In addition, inflammasome assembly and activation seems to be due to the loss of phagolysosomal integrity, which both allows for the assembly of NLRP3 and facilitates the direct binding of double-stranded *Pf* gDNA to AIM2. This model of innate immune activation is predicated on the belief that DNA dissociates from Hz (or is released from dying parasites) in the phagolysosome and ultimately gains access to the cytosol. In fact, this is what we observed: gDNA from *Plasmodium* was stained with DAPI and bound overnight to serum-coated sHz. These sHz/*Pf* gDNA complexes were fed to macrophages and followed by confocal microscopy over time. As shown in Figure 5F, both free DNA and Hz could be found outside the lysosomal compartment. This result confirms that Hz is responsible for delivering DNA to the cytosol, where DNA can activate cytosolic DNA receptors. In addition to AIM2, cytosolic DNA sensors can also trigger the production of type I INFs under these conditions.

Plasmodium-Infected Erythrocytes Induce IL-1β Production via Both the NLRP3 and AIM2 Inflammasomes, Similarly to DNA-Coated sHz

Peripheral smears of patients with high parasitemia malaria often reveal the presence of Hz in phagocytes. This intracellular Hz is presumably due to the phagocytosis and degradation of parasites that contain Hz (Bettiol et al., 2010; Ing et al., 2006; McGilvray et al., 2000) in addition to the uptake of any free Hz or digestive vacuoles that may be in the vasculature. iRBCs often have visible Hz within them when stained with Giemsa. We hypothesized that if the Hz that is present in iRBCs is truly a major immune activator, the innate immune-activating activity of phagocytosed iRBCs should resemble that of purified nHz or sHz that is experimentally coated with plasmodial gDNA.

To visualize the uptake of iRBCs by macrophages, we fed macrophages RBCs infected with fluorescent *P. berghei* NK65 (Figure 6A). These iRBCs were fully competent to activate IL-1β production from unprimed macrophages (Figure 6B). As was the case with sHz/CpG (Figure 3F), this process was inhibited by blocking phagolysosomal acidification with bafilomycin A (Figure 6B). Hz could be seen within phagocytosed iRBCs and induced phagolysosomal destabilization (Figure S6A). Like sHz/CpG or nHz (Figures 1E and 5A, respectively), iRBCs triggered the formation of ASC specks in the cytosol of ASC-CFP macrophages (Figures 6C and S6B). Uninfected RBCs (uRBCs) did not induce the formation of ASC pyroptosomes (data not shown). Similar to what was observed for sHz/gDNA and nHz, the speck assay revealed AIM2 activation by iRBCs. When we prestained parasites with the nucleic acid stain DAPI and then cocultured iRBCs with AIM2-citrine macrophages, was observed AIM2 assembly. In fact, DAPI-stained DNA actually colocalized with the AIM2 inflammasome (Figures 6D, bottom panel, and S6C).

We next exposed WT and TLR9 knockout macrophages to infected RBCs and measured IL-1β production. WT BMDMs responded robustly to infected RBCs in the absence of a priming step. The priming step, in fact, appeared to be TLR9 dependent (Figure 6E), and iRBCs induced TLR9 translocation (data not shown). When we tested macrophages from *Nlrp3*$^{-/-}$ (Figure 6F, upper-right panel) and *Aim2*$^{-/-}$ (Figure 6F, lower-middle panel)

(E) Confocal microscopy of NLRP3-citrine macrophages untreated or treated with sHz/CpG (5 μg/ml), sHz/*Pf* gDNA (4 μg/ml), or nigericin, or transfected with 100 ng/ml *Pf* gDNA using Lipofectamine. Images are representative of at least ten fields of view and three independent experiments. Scale bars, all 20 μm except the one at the bottom, which is 5 μm.
See also Figure S4.

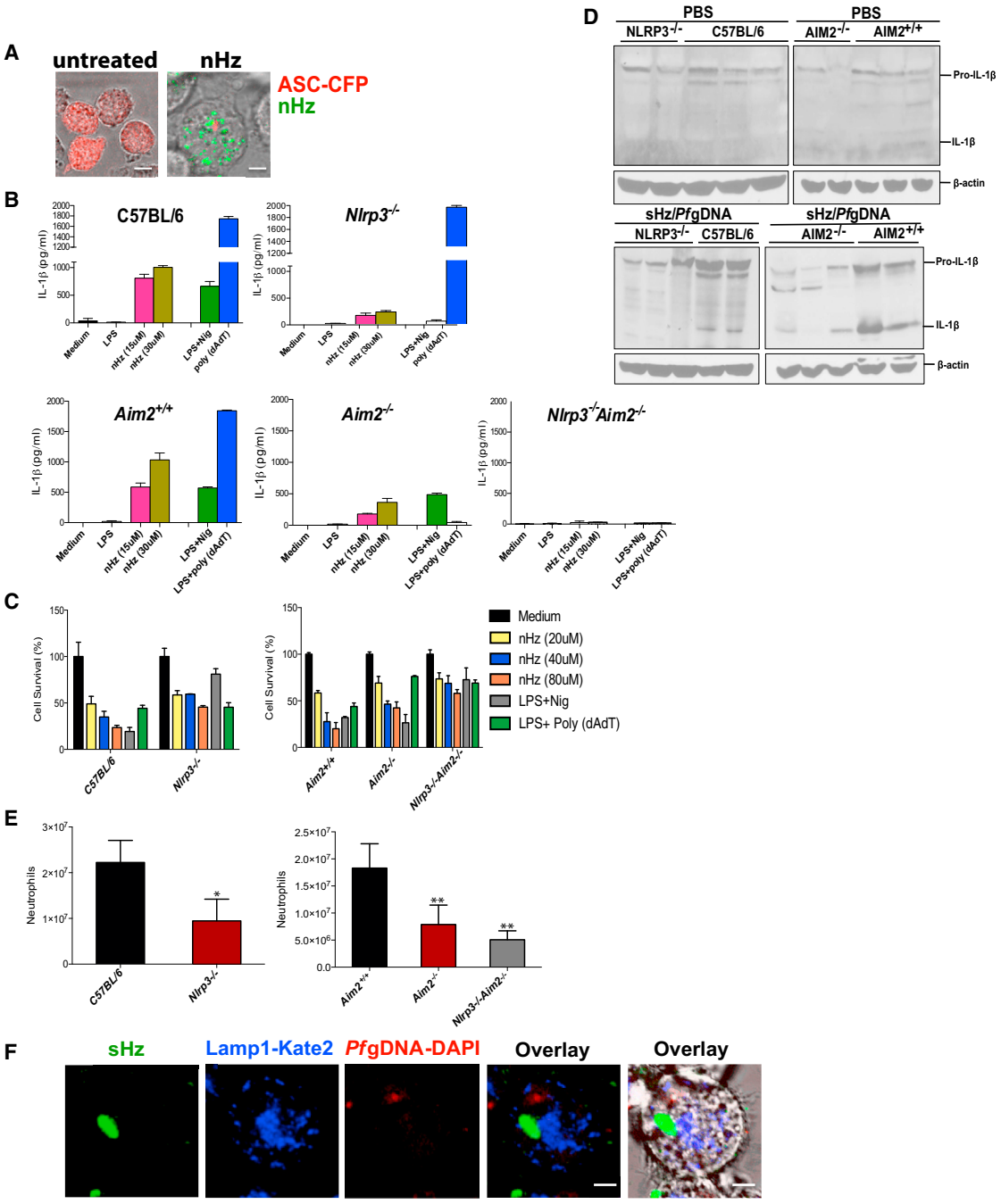

Figure 5. nHz and sHz/*Pf* gDNA Complex Induce IL-1β Production and Pyroptosis Both In Vitro and In Vivo via NLRP3 and AIM2

(A) Macrophages stably expressing ASC-CFP were left untreated or treated with nHz (100 μM). The formation of ASC pyroptosomes was visualized by confocal microscopy. Scale bars, 15 μm (left) and 5 μm (right).

(B) Primary WT, *Nlrp3*$^{-/-}$, *Aim2*$^{+/+}$, *Aim2*$^{-/-}$, and *Nlrp3*$^{-/-}$*Aim2*$^{-/-}$ BMDMs were incubated for 12 hr with 15 μM and 30 μM of nHz, or nigericin (10 μM), or transfected with 1.5 μg/ml poly (dAdT) using Lipofectamine. Cell culture supernatants were assessed for IL-1β release by ELISA.

(C) Primary WT, *Nlrp3*$^{-/-}$, *Aim2*$^{+/+}$, *Aim2*$^{-/-}$, and *Nlrp3*$^{-/-}$*Aim2*$^{-/-}$ BMDMs were incubated for 12 hr with 20 μM, 40 μM, and 80 μM of nHz or transfected with Poly (dAdT). Cell survival was measured using calcein AM. The medium was set as 100%. Data are mean cytokine levels ± SD of triplicate determinations and are representative of three independent experiments.

(D) WT, *Nlrp3*$^{-/-}$, *Aim2*$^{+/+}$, *Aim2*$^{-/-}$ and *Nlrp3*$^{-/-}$*Aim2*$^{-/-}$ mice were i.v. injected in the tail vein with endotoxin-free PBS or sHz/*Pf* gDNA (1 mg sHz, 15 μg *Pf* gDNA). After 12 hr, the livers were dissected and homogenized. Each lane corresponds to one mouse.

(E) WT (n = 12), *Nlrp3*$^{-/-}$ (n = 16), *Aim2*$^{+/+}$ (n = 9), *Aim2*$^{-/-}$ (n = 14), and *Nlrp3*$^{-/-}$*Aim2*$^{-/-}$ (n = 6) mice were intraperitoneally injected with sHz/*Pf* gDNA (1 mg sHz, 15 μg *Pf* gDNA) or PBS. After 15 hr, peritoneal cells were harvested and counted, and FACS analysis was performed using GR-1 antibody. Basal neutrophil influx

(legend continued on next page)

mice, we observed a markedly decreased response compared with their littermate controls. No response was observed in the *Nlrp3*$^{-/-}$*Aim2*$^{-/-}$ double-knockout cells (Figure 6F, lower-right panel). Hence, in all respects, the characteristics of macrophage stimulation by infected erythrocytes resembled those of *Pf* gDNA-coated sHz or nHz.

DISCUSSION

Malaria remains one of the most important infectious diseases in the world today. The disease is typically characterized by recurrent febrile paroxysms that are attributed to circulating proinflammatory cytokines released in response to the parasite components (Adachi et al., 2001; Pichyangkul et al., 1994; Sherry et al., 1995; Taramelli et al., 1998). Malaria is a complicated disease in which many parasite and host components contribute to disease severity. Nevertheless, understanding the details of the innate host response is truly important because the details of the cytokine response have the potential to lead to translational breakthroughs. The current data set, for example, raises the possibility that immunomodulation of the NLRP3 and AIM2 inflammasomes' activity might be therapeutic.

As we learn more about inflammation in malaria, Hz is surprisingly emerging as a key component of almost every aspect of innate immune activation. We previously suggested that Hz acts as a delivery agent, introducing DNA into the lysosomal compartment. Yet, as we have shown here, Hz does much more than help DNA engage TLR9, as it is essential for activation of NLRP3, AIM2, and even (by extrapolation) the type I INF response that occurs in the cytosol of immune cells. This overall scheme of innate immune activation in malaria is diagrammed in Figure S6D.

One question that requires more mechanistic study is how DNA might actually colocalize with Hz in infected erythrocytes, considering that Hz is normally in the food vacuole of the parasite. One possibility is that during the process of parasite expansion, there is constant turnover of a subpopulation of parasites, and that during this process of parasite turnover, Hz may be exposed to parasite DNA. Indeed, a recent paper by Love et al. (2012) provided evidence that this occurs as the result of human platelet factor 4, which kills plasmodium inside erythrocytes by selectively lysing the parasite digestive vacuole, ultimately killing the parasite. It is clear that as the parasite nucleus undergoes karyolysis, plasmodial DNA and Hz can mix in the cytosol.

As confirmed here, Hz is a potent activator of the NLRP3 inflammasome (Dostert et al., 2009; Griffith et al., 2009; Reimer et al., 2010; Shio et al., 2009). Because the NLRP3 inflammasome is a potential source of large quantities of mature IL-1β, this role of Hz must be considered to be quite important. Indeed, along with TNFα, IL-1β has been recognized as one of the cytokines most closely associated with death during malaria (Day et al., 1999; Kwiatkowski et al., 1990; Prakash et al., 2006; Vogetseder et al., 2004). The pleiotropic effects of IL-1β might explain some discrepancies between our results and those of Jaramillo et al. (2009), especially in vivo, where sHz would be expected to induce the production of IL-1β (and IL-18) from the liver in the absence of priming. Perhaps even more important than the role of Hz in activating the NLRP3 inflammasome, Hz has a destabilizing activity on the integrity of the phagolysosome. The result of this activity is to allow phagolysosomal components access to the cytosol. The integrity of the cytosol is of paramount importance for immune cells, and the subsequent widespread activation of the innate immune system is not surprising.

nHz contains abundant proteins associated with the crystal (Ashong et al., 1989; Goldie et al., 1990), and the effects of these proteins remain to be fully defined. The present report does not rule out an important role for these proteins, as the work was relatively narrow in its focus on DNA. For example, it has been reported that host serum fibrinogen, which is stably bound to Hz, strongly increases the capacity of nHz to activate monocyte inflammatory functions (Barrera et al., 2011). Indeed, Hz-, DNA-, and host-associated proteins could potentially form a complex and augment innate immune responses.

The demonstration of innate immune activation in human patients lags far behind what we have learned from in vitro modeling of the innate immune response in tissue culture, and in vivo modeling in rodents. Close biochemical and immunological studies of innate immune responses in patients are complicated by the inaccessibility of certain important tissues (e.g., human spleens, livers, and brains) that obviously cannot be harvested during the course of illness. Hence, we are reliant upon mouse models and the examination of peripheral cells to make educated guesses about what is happening in severe disease. This is an important effort, because if the world is to develop effective immunomodulatory remedies for life-threatening disease, as well as a truly effective malaria vaccine, dramatic improvements in our understanding of the biology of inflammation during malaria are necessary.

EXPERIMENTAL PROCEDURES

Mice

C57BL/6, *Nlrp3*$^{-/-}$, *Nlrp6*$^{-/-}$, and *Nlrp12*$^{-/-}$ mice were purchased from The Jackson Laboratory. *Asc*$^{-/-}$ (Pycard$^{-/-}$) mice were provided by Millennium Pharmaceuticals. Caspase-1-deficient mice (*Casp1*$^{-/-}$) were provided by A. Hise (Case Western Reserve), *Ctsb*$^{-/-}$ mice were provided by T. Reinheckel (University of Freiburg), and *Ctsl*$^{-/-}$ mice were provided by H. Ploegh (MIT). *Aim2*$^{+/+}$ and *Aim2*$^{-/-}$ mice were generated as described in Rathinam et al. (2010). *Tlr9*$^{-/-}$ mice were a gift of S. Akira (Osaka University). UNC93B1 mutant (3d) mice were provided by B. Beutler (University of Texas Southwestern). Mice 6–8 weeks of age were used in all experiments. All mouse strains were bred and maintained under specific pathogen-free conditions at the University of Massachusetts Medical School.

in PBS-injected mice was subtracted to determine the total number of neutrophils that were recruited to the peritoneal cavity. Student's t test was used to calculate p values (*$p < 0.05$, **$p < 0.001$).

(F) *Pf* gDNA (5 μg/ml) was DAPI stained for 30 min and used to make sHz/*Pf* gDNA. Lamp1-Kate2 macrophages were then stimulated with sHz/*Pf* gDNA for 2 hr and subjected to reflection confocal microscopy. Fields are representative of at least ten fields of view and three independent experiments. Scale bar, 5 μm. See also Figure S5.

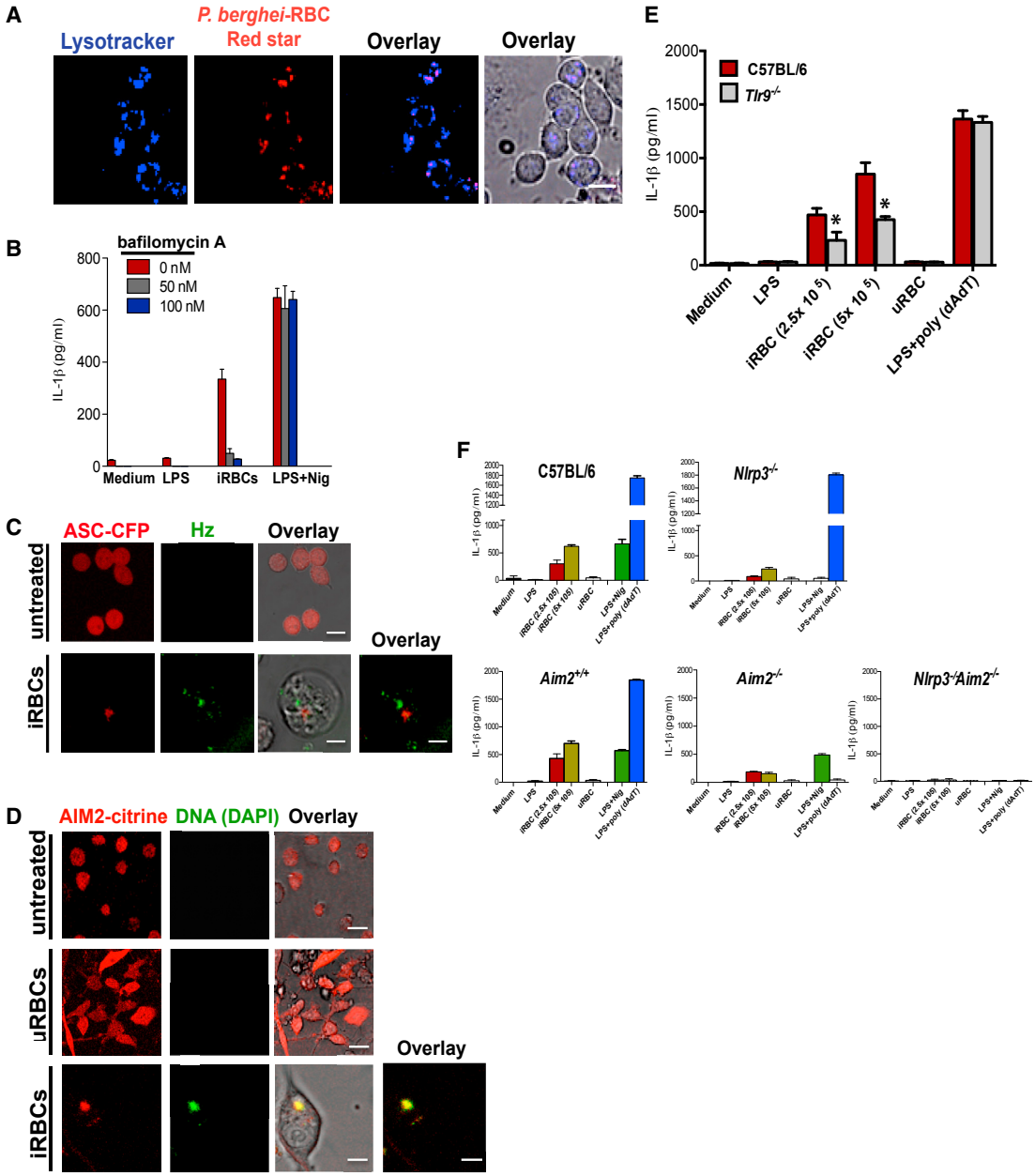

Figure 6. iRBC-Induced IL-1β Production Is NLRP3 and AIM2 Dependent

(A) Confocal imaging of immortalized BMDMs incubated with 8 × 10^5 *P. berghei* (NK65) Red star for 2 hr. Lysosomes were stained with LysoTracker (blue). Scale bar, 20 μm.

(B) ELISA of the release of IL-1β from immortalized BMDMs pretreated with indicated concentrations of bafilomycin A for 2 hr and then incubated with 8 × 10^5 iRBCs for 12 hr.

(C) ASC-CFP macrophages were incubated with 8 × 10^5 iRBCs for 12 hr and imaged by confocal microscopy. nHz was visualized by reflection microscopy (green). Scale bars, 20 μm (top) and 5 μm (bottom).

(D) iRBCs and uRBCs were incubated with DAPI for 1 hr and then cocultured with AIM2-citrine macrophages for 2 hr. Fields are representative of at least ten fields of view and three independent experiments. Scale bars, 20 μm (top), 20 μm (middle), and 5 μm (bottom).

(E) WT and *Tlr9*$^{-/-}$ BMDMs were incubated with 2.5 × 10^5 and 5 × 10^5 iRBCs or 5 × 10^5 uRBCs, or transfected with poly (dAdT) using Lipofectamine for 12 hr. The supernatants were subjected to ELISA for IL-1β. *$p < 0.05$, Student's t test.

(F) Primary WT, *NLRP3*$^{-/-}$, *AIM2*$^{+/+}$, *AIM2*$^{-/-}$, and *NLRP3*$^{-/-}$*AIM2*$^{-/-}$ BMDMs were incubated with 2.5 × 10^5 and 5 × 10^5 iRBCs or 5 × 10^5 uRBCs for 12 hr, or transfected with poly (dAdT) using Lipofectamine. The supernatants were subjected to ELISA for IL-1β. iRBCs used for all experiments above were taken at day 14 from C57BL/6 mice infected with *P. berghei* NK65. Data are presented as the mean of triplicate determinations ± SD and are representative of three independent experiments.

See also Figure S6.

Reagents

Lipofectamine 2000 was obtained from Invitrogen. Poly (dAdT), cytochalasin D, pepstain A, acridine orange, and BrdU were obtained from Sigma-Aldrich. Bafilomycin A1 and Giemsa stain were obtained from Fluka Analytical. Alexa Fluor 546-conjugated dextran, LysoTracker, Cell Mask Plasma membrane stain, DAPI, SYTO 60, calcein AM, and propidium iodide were obtained from Molecular Probes/Invitrogen. Nigericin was obtained from Invivogen. CA-074Me was obtained from Enzo LifeSciences. Cat L inhibitor was obtained from Calbiochem. Uricase (Elitek) was obtained from Sanofi-Aventis. Dulbecco's modified Eagle's medium (DMEM) was obtained from Cellgro, and low endotoxin FBS was obtained from Atlas Biologicals. CpG DNA ODN 1826, CpG-Alexa 647, and AT2-A647 were obtained from IDT. *Pf* 3D7 gDNA was purified as described previously (Parroche et al., 2007). *Pf* HB3_B2, *Pf* T9/94, and *Pf* Dd2 gDNA was obtained from the Malaria Research and Reference Resource Center at NIAID.

Confocal Microscopy and Flow Cytometry

Confocal reflection microscopy was combined with fluorescence microscopy as described in Hornung et al., (2008) on a Leica TCS SP8 AOBS confocal laser-scanning microscope. Flow cytometry was performed as described in Hornung et al., (2008).

Cell Culture, Stimulations, ELISA, and Immunoblot Analysis

Immortalized macrophage cell lines were generated from WT, *NLRP3*$^{-/-}$, *ASC*$^{-/-}$, *caspase1*$^{-/-}$, *TLR9*$^{-/-}$, *ctsb*$^{-/-}$, *ctsl*$^{-/-}$, and 3d mice (Hornung et al., 2008). Primary BMDMs were generated as described previously (Rathinam et al., 2010). Human PBMCs were isolated from whole blood of healthy volunteers by density gradient centrifugation. All cells, primary BMDMs, and cell lines were cultured in DMEM supplemented with ciprofloxacin and 10% FBS. For all experiments for immunoblot analysis, serum-free DMEM medium was used. For stimulations, poly (dAdT) (1.5 μg/ml) or gDNA was transfected with Lipofectamine 2000 (Invitrogen). Nigericin (10 μM) was added 1 hr before supernatants were collected. The next day, 2×10^5 macrophages were plated and stimulated with the indicated amounts of CpG, sHz, nHz, sHz/CpG and sHz/*Pf* gDNA, iRBCs, and RBCs. Cytokine measurements were performed using ELISA kits for mouse IL-1β and TNFα (R&D Systems). Immunoblot analysis was performed with anti-mouse IL-1β antibody (AF-401-NA; R&D Systems) and rabbit anti-goat immunoglobulin G horseradish peroxidase (Santa Cruz Biotechnology).

Culture of Parasites and Preparation of sHz, nHz, sHz/CpG DNA, and sHz/*Pf* gDNA

sHz was prepared using hemin chloride (>98% pure by high-performance liquid chromatography; Sigma) as previously described (Shio et al., 2009). The dried pigment was suspended in endotoxin-free PBS (Cellgro) and inspected by microscopy for size and other characteristics. The crystalline nature of the crystals was confirmed by reflection confocal microscopy and electron microscopy (Figure S1B). *Pf* parasites (3D7 strain) were cultured as previously described (Parroche et al., 2007). *Pf* culture stages and parasitemia levels were assessed daily by Giemsa staining and also checked routinely for Mycoplasma. nHz was extracted from the parasite cultures as described in Parroche et al. (2007). The dried pigment was suspended in endotoxin-free PBS and stored at 4°C. sHz/CpG complexes were prepared by incubating sHz and CpG in a rocker for 2 hr and washing the complex three times with PBS. sHz/*Pf* gDNA was prepared by coating sHz with FBS (Atlas Biologicals) overnight and then incubating with *Pf* gDNA for 2 hr, followed by three washes with PBS.

Infection of Mice

P. berghei (NK65) Red star, *P. berghei* (Pb) NK65, and *P. berghei* (Pb) ANKA were obtained from the Malaria Research and Reference Resource Center (MR4) and maintained by passage in BALB/c mice. The parasitemia level was assessed every 3 days by microscopic examination of Giemsa-stained smears of blood.

In Vivo Labeling of *Plasmodium* with BrdU

C57BL/6 mice infected with *P. berghei* ANKA were injected daily intraperitoneally with 1 mg of BrdU in 1 ml of PBS on days 9, 10, and 11 postinfection. Blood was harvested by cardiac puncture on day 12. Blood was washed several times and 1 ml of mouse blood was layered onto 1 ml of Mono-Poly Resolving Medium and centrifuged for 45 min at 3,000 rpm. After centrifugation, RBCs in the bottom layer were collected, washed, and resuspended in PBS. RBC suspensions were subsequently loaded into an LS column (Miltenyi Biotec) and placed into a MACS separator. The flow-through (devoid of free Hz) was collected and loaded onto an LD column (Miltenyi Biotec). When removed from the magnetic field, the subsequent flow-through contained ~99% *Plasmodium*-infected erythrocytes. BMDMs were incubated with iRBCs for various time periods, fixed using ice-cold 70% ethanol, and then incubated with 2 M HCl for 30 min at room temperature. Cells were washed two times with PBS, incubated with FITC-conjugated BrdU antibody (eBiosciences) for 2 hr in the dark, and subjected to confocal microscopy.

SUPPLEMENTAL INFORMATION

Supplemental Information includes six figures and can be found with this article online at http://dx.doi.org/10.1016/j.celrep.2013.12.014.

AUTHOR CONTRIBUTIONS

K.A.F., D.T.G., and R.T.G. oversaw the whole project. P.K. designed and conducted the experiments with help from R.D., J.C., A.S., and V.R. Preparation of nHz was done by Y.C., P.K., K.A.F., and D.T.G. wrote the manuscript.

ACKNOWLEDGMENTS

The authors thank Anna Cerny for animal husbandry, and Drs. Shizuo Akira, Bruce Beutler, and Hidde Pleogh (Massachusetts Institutes of Technology, Boston) for transgenic mice. This work was supported by NIH grants AI067497 (to K.A.F.), AI079293 (to K.A.F. and D.T.G.), and R21AI80907 (to R.T.G.).

Received: July 7, 2013
Revised: November 12, 2013
Accepted: December 10, 2013
Published: January 2, 2014

REFERENCES

Adachi, K., Tsutsui, H., Kashiwamura, S., Seki, E., Nakano, H., Takeuchi, O., Takeda, K., Okumura, K., Van Kaer, L., Okamura, H., et al. (2001). Plasmodium berghei infection in mice induces liver injury by an IL-12- and toll-like receptor/myeloid differentiation factor 88-dependent mechanism. J. Immunol. *167*, 5928–5934.

Arthur, J.C., Lich, J.D., Ye, Z., Allen, I.C., Gris, D., Wilson, J.E., Schneider, M., Roney, K.E., O'Connor, B.P., Moore, C.B., et al. (2010). Cutting edge: NLRP12 controls dendritic and myeloid cell migration to affect contact hypersensitivity. J. Immunol. *185*, 4515–4519.

Ashong, J.O., Blench, I.P., and Warhurst, D.C. (1989). The composition of haemozoin from Plasmodium falciparum. Trans. R. Soc. Trop. Med. Hyg. *83*, 167–172.

Barrera, V., Skorokhod, O.A., Baci, D., Gremo, G., Arese, P., and Schwarzer, E. (2011). Host fibrinogen stably bound to hemozoin rapidly activates monocytes via TLR-4 and CD11b/CD18-integrin: a new paradigm of hemozoin action. Blood *117*, 5674–5682.

Bauernfeind, F.G., Horvath, G., Stutz, A., Alnemri, E.S., MacDonald, K., Speert, D., Fernandes-Alnemri, T., Wu, J., Monks, B.G., Fitzgerald, K.A., et al. (2009). Cutting edge: NF-kappaB activating pattern recognition and cytokine receptors license NLRP3 inflammasome activation by regulating NLRP3 expression. J. Immunol. *183*, 787–791.

Bettiol, E., Van de Hoef, D.L., Carapau, D., and Rodriguez, A. (2010). Efficient phagosomal maturation and degradation of Plasmodium-infected erythrocytes by dendritic cells and macrophages. Parasite Immunol. *32*, 389–398.

Brown, H., Turner, G., Rogerson, S., Tembo, M., Mwenechanya, J., Molyneux, M., and Taylor, T. (1999). Cytokine expression in the brain in human cerebral malaria. J. Infect. Dis. *180*, 1742–1746.

Bürckstümmer, T., Baumann, C., Blüml, S., Dixit, E., Dürnberger, G., Jahn, H., Planyavsky, M., Bilban, M., Colinge, J., Bennett, K.L., and Superti-Furga, G. (2009). An orthogonal proteomic-genomic screen identifies AIM2 as a cytoplasmic DNA sensor for the inflammasome. Nat. Immunol. *10*, 266–272.

Clark, I.A., and Rockett, K.A. (1994). The cytokine theory of human cerebral malaria. Parasitol. Today (Regul. Ed.) *10*, 410–412.

Clark, I.A., Cowden, W.B., and Rockett, K.A. (1994). The pathogenesis of human cerebral malaria. Parasitol. Today (Regul. Ed.) *10*, 417–418.

Coban, C., Ishii, K.J., Kawai, T., Hemmi, H., Sato, S., Uematsu, S., Yamamoto, M., Takeuchi, O., Itagaki, S., Kumar, N., et al. (2005). Toll-like receptor 9 mediates innate immune activation by the malaria pigment hemozoin. J. Exp. Med. *201*, 19–25.

Day, N.P., Hien, T.T., Schollaardt, T., Loc, P.P., Chuong, L.V., Chau, T.T., Mai, N.T., Phu, N.H., Sinh, D.X., White, N.J., and Ho, M. (1999). The prognostic and pathophysiologic role of pro- and antiinflammatory cytokines in severe malaria. J. Infect. Dis. *180*, 1288–1297.

Dostert, C., Guarda, G., Romero, J.F., Menu, P., Gross, O., Tardivel, A., Suva, M.L., Stehle, J.C., Kopf, M., Stamenkovic, I., et al. (2009). Malarial hemozoin is a Nalp3 inflammasome activating danger signal. PLoS ONE *4*, e6510.

Duewell, P., Kono, H., Rayner, K.J., Sirois, C.M., Vladimer, G., Bauernfeind, F.G., Abela, G.S., Franchi, L., Nuñez, G., Schnurr, M., et al. (2010). NLRP3 inflammasomes are required for atherogenesis and activated by cholesterol crystals. Nature *464*, 1357–1361.

Elinav, E., Strowig, T., Kau, A.L., Henao-Mejia, J., Thaiss, C.A., Booth, C.J., Peaper, D.R., Bertin, J., Eisenbarth, S.C., Gordon, J.I., and Flavell, R.A. (2011). NLRP6 inflammasome regulates colonic microbial ecology and risk for colitis. Cell *145*, 745–757.

Franklin, B.S., Parroche, P., Ataíde, M.A., Lauw, F., Ropert, C., de Oliveira, R.B., Pereira, D., Tada, M.S., Nogueira, P., da Silva, L.H., et al. (2009). Malaria primes the innate immune response due to interferon-gamma induced enhancement of toll-like receptor expression and function. Proc. Natl. Acad. Sci. USA *106*, 5789–5794.

Gardner, M.J., Hall, N., Fung, E., White, O., Berriman, M., Hyman, R.W., Carlton, J.M., Pain, A., Nelson, K.E., Bowman, S., et al. (2002). Genome sequence of the human malaria parasite Plasmodium falciparum. Nature *419*, 498–511.

Gazzinelli, R.T., and Denkers, E.Y. (2006). Protozoan encounters with Toll-like receptor signalling pathways: implications for host parasitism. Nat. Rev. Immunol. *6*, 895–906.

Goldie, P., Roth, E.F., Jr., Oppenheim, J., and Vanderberg, J.P. (1990). Biochemical characterization of Plasmodium falciparum hemozoin. Am. J. Trop. Med. Hyg. *43*, 584–596.

Gowda, N.M., Wu, X., and Gowda, D.C. (2011). The nucleosome (histone-DNA complex) is the TLR9-specific immunostimulatory component of Plasmodium falciparum that activates DCs. PLoS ONE *6*, e20398.

Grau, G.E., Heremans, H., Piguet, P.F., Pointaire, P., Lambert, P.H., Billiau, A., and Vassalli, P. (1989). Monoclonal antibody against interferon gamma can prevent experimental cerebral malaria and its associated overproduction of tumor necrosis factor. Proc. Natl. Acad. Sci. USA *86*, 5572–5574.

Griffith, J.W., Sun, T., McIntosh, M.T., and Bucala, R. (2009). Pure Hemozoin is inflammatory in vivo and activates the NALP3 inflammasome via release of uric acid. J. Immunol. *183*, 5208–5220.

Guermonprez, P., Helft, J., Claser, C., Deroubaix, S., Karanje, H., Gazumyan, A., Darasse-Jèze, G., Telerman, S.B., Breton, G., Schreiber, H.A., et al. (2013). Inflammatory Flt3l is essential to mobilize dendritic cells and for T cell responses during Plasmodium infection. Nat. Med. *19*, 730–738.

Halle, A., Hornung, V., Petzold, G.C., Stewart, C.R., Monks, B.G., Reinheckel, T., Fitzgerald, K.A., Latz, E., Moore, K.J., and Golenbock, D.T. (2008). The NALP3 inflammasome is involved in the innate immune response to amyloid-beta. Nat. Immunol. *9*, 857–865.

Hornung, V., Bauernfeind, F., Halle, A., Samstad, E.O., Kono, H., Rock, K.L., Fitzgerald, K.A., and Latz, E. (2008). Silica crystals and aluminum salts activate the NALP3 inflammasome through phagosomal destabilization. Nat. Immunol. *9*, 847–856.

Hornung, V., Ablasser, A., Charrel-Dennis, M., Bauernfeind, F., Horvath, G., Caffrey, D.R., Latz, E., and Fitzgerald, K.A. (2009). AIM2 recognizes cytosolic dsDNA and forms a caspase-1-activating inflammasome with ASC. Nature *458*, 514–518.

Ing, R., Segura, M., Thawani, N., Tam, M., and Stevenson, M.M. (2006). Interaction of mouse dendritic cells and malaria-infected erythrocytes: uptake, maturation, and antigen presentation. J. Immunol. *176*, 441–450.

Jaramillo, M., Godbout, M., and Olivier, M. (2005). Hemozoin induces macrophage chemokine expression through oxidative stress-dependent and -independent mechanisms. J. Immunol. *174*, 475–484.

Jaramillo, M., Bellemare, M.J., Martel, C., Shio, M.T., Contreras, A.P., Godbout, M., Roger, M., Gaudreault, E., Gosselin, J., Bohle, D.S., and Olivier, M. (2009). Synthetic Plasmodium-like hemozoin activates the immune response: a morphology-function study. PLoS ONE *4*, e6957.

Kwiatkowski, D., and Nowak, M. (1991). Periodic and chaotic host-parasite interactions in human malaria. Proc. Natl. Acad. Sci. USA *88*, 5111–5113.

Kwiatkowski, D., Hill, A.V., Sambou, I., Twumasi, P., Castracane, J., Manogue, K.R., Cerami, A., Brewster, D.R., and Greenwood, B.M. (1990). TNF concentration in fatal cerebral, non-fatal cerebral, and uncomplicated Plasmodium falciparum malaria. Lancet *336*, 1201–1204.

Last-Barney, K., Homon, C.A., Faanes, R.B., and Merluzzi, V.J. (1988). Synergistic and overlapping activities of tumor necrosis factor-alpha and IL-1. J. Immunol. *141*, 527–530.

Latz, E., Schoenemeyer, A., Visintin, A., Fitzgerald, K.A., Monks, B.G., Knetter, C.F., Lien, E., Nilsen, N.J., Espevik, T., and Golenbock, D.T. (2004). TLR9 signals after translocating from the ER to CpG DNA in the lysosome. Nat. Immunol. *5*, 190–198.

Lopera-Mesa, T.M., Mita-Mendoza, N.K., van de Hoef, D.L., Doumbia, S., Konaté, D., Doumbouya, M., Gu, W., Traoré, K., Diakité, S.A., Remaley, A.T., et al. (2012). Plasma uric acid levels correlate with inflammation and disease severity in Malian children with Plasmodium falciparum malaria. PLoS ONE *7*, e46424.

Love, M.S., Millholland, M.G., Mishra, S., Kulkarni, S., Freeman, K.B., Pan, W., Kavash, R.W., Costanzo, M.J., Jo, H., Daly, T.M., et al. (2012). Platelet factor 4 activity against P. falciparum and its translation to nonpeptidic mimics as antimalarials. Cell Host Microbe *12*, 815–823.

Mariathasan, S., Newton, K., Monack, D.M., Vucic, D., French, D.M., Lee, W.P., Roose-Girma, M., Erickson, S., and Dixit, V.M. (2004). Differential activation of the inflammasome by caspase-1 adaptors ASC and Ipaf. Nature *430*, 213–218.

Martinon, F., Pétrilli, V., Mayor, A., Tardivel, A., and Tschopp, J. (2006). Gout-associated uric acid crystals activate the NALP3 inflammasome. Nature *440*, 237–241.

McGilvray, I.D., Serghides, L., Kapus, A., Rotstein, O.D., and Kain, K.C. (2000). Nonopsonic monocyte/macrophage phagocytosis of Plasmodium falciparum-parasitized erythrocytes: a role for CD36 in malarial clearance. Blood *96*, 3231–3240.

Orengo, J.M., Evans, J.E., Bettiol, E., Leliwa-Sytek, A., Day, K., and Rodriguez, A. (2008). Plasmodium-induced inflammation by uric acid. PLoS Pathog. *4*, e1000013.

Orengo, J.M., Leliwa-Sytek, A., Evans, J.E., Evans, B., van de Hoef, D., Nyako, M., Day, K., and Rodriguez, A. (2009). Uric acid is a mediator of the Plasmodium falciparum-induced inflammatory response. PLoS ONE *4*, e5194.

Parroche, P., Lauw, F.N., Goutagny, N., Latz, E., Monks, B.G., Visintin, A., Halmen, K.A., Lamphier, M., Olivier, M., Bartholomeu, D.C., et al. (2007). Malaria hemozoin is immunologically inert but radically enhances innate responses by presenting malaria DNA to Toll-like receptor 9. Proc. Natl. Acad. Sci. USA *104*, 1919–1924.

Pichyangkul, S., Saengkrai, P., and Webster, H.K. (1994). Plasmodium falciparum pigment induces monocytes to release high levels of tumor necrosis factor-alpha and interleukin-1 beta. Am. J. Trop. Med. Hyg. *51*, 430–435.

Pichyangkul, S., Yongvanitchit, K., Kum-arb, U., Hemmi, H., Akira, S., Krieg, A.M., Heppner, D.G., Stewart, V.A., Hasegawa, H., Looareesuwan, S., et al. (2004). Malaria blood stage parasites activate human plasmacytoid dendritic cells and murine dendritic cells through a Toll-like receptor 9-dependent pathway. J. Immunol. *172*, 4926–4933.

Prakash, D., Fesel, C., Jain, R., Cazenave, P.A., Mishra, G.C., and Pied, S. (2006). Clusters of cytokines determine malaria severity in Plasmodium falciparum-infected patients from endemic areas of Central India. J. Infect. Dis. *194*, 198–207.

Rathinam, V.A., Jiang, Z., Waggoner, S.N., Sharma, S., Cole, L.E., Waggoner, L., Vanaja, S.K., Monks, B.G., Ganesan, S., Latz, E., et al. (2010). The AIM2 inflammasome is essential for host defense against cytosolic bacteria and DNA viruses. Nat. Immunol. *11*, 395–402.

Reimer, T., Shaw, M.H., Franchi, L., Coban, C., Ishii, K.J., Akira, S., Horii, T., Rodriguez, A., and Núñez, G. (2010). Experimental cerebral malaria progresses independently of the Nlrp3 inflammasome. Eur. J. Immunol. *40*, 764–769.

Sharma, S., DeOliveira, R.B., Kalantari, P., Parroche, P., Goutagny, N., Jiang, Z., Chan, J., Bartholomeu, D.C., Lauw, F., Hall, J.P., et al. (2011). Innate immune recognition of an AT-rich stem-loop DNA motif in the Plasmodium falciparum genome. Immunity *35*, 194–207.

Sherry, B.A., Alava, G., Tracey, K.J., Martiney, J., Cerami, A., and Slater, A.F. (1995). Malaria-specific metabolite hemozoin mediates the release of several potent endogenous pyrogens (TNF, MIP-1 alpha, and MIP-1 beta) in vitro, and altered thermoregulation in vivo. J. Inflamm. *45*, 85–96.

Shio, M.T., Eisenbarth, S.C., Savaria, M., Vinet, A.F., Bellemare, M.J., Harder, K.W., Sutterwala, F.S., Bohle, D.S., Descoteaux, A., Flavell, R.A., and Olivier, M. (2009). Malarial hemozoin activates the NLRP3 inflammasome through Lyn and Syk kinases. PLoS Pathog. *5*, e1000559.

Snow, R.W., Guerra, C.A., Noor, A.M., Myint, H.Y., and Hay, S.I. (2005). The global distribution of clinical episodes of Plasmodium falciparum malaria. Nature *434*, 214–217.

Stashenko, P., Dewhirst, F.E., Peros, W.J., Kent, R.L., and Ago, J.M. (1987). Synergistic interactions between interleukin 1, tumor necrosis factor, and lymphotoxin in bone resorption. J. Immunol. *138*, 1464–1468.

Tabeta, K., Hoebe, K., Janssen, E.M., Du, X., Georgel, P., Crozat, K., Mudd, S., Mann, N., Sovath, S., Goode, J., et al. (2006). The Unc93b1 mutation 3d disrupts exogenous antigen presentation and signaling via Toll-like receptors 3, 7 and 9. Nat. Immunol. *7*, 156–164.

Taramelli, D., Basilico, N., De Palma, A.M., Saresella, M., Ferrante, P., Mussoni, L., and Olliaro, P. (1998). The effect of synthetic malaria pigment (beta-haematin) on adhesion molecule expression and interleukin-6 production by human endothelial cells. Trans. R. Soc. Trop. Med. Hyg. *92*, 57–62.

van de Hoef, D.L., Coppens, I., Holowka, T., Ben Mamoun, C., Branch, O., and Rodriguez, A. (2013). Plasmodium falciparum-derived uric acid precipitates induce maturation of dendritic cells. PLoS ONE *8*, e55584.

Vogetseder, A., Ospelt, C., Reindl, M., Schober, M., and Schmutzhard, E. (2004). Time course of coagulation parameters, cytokines and adhesion molecules in Plasmodium falciparum malaria. Trop. Med. Int. Health *9*, 767–773.

Comprehensive Supplemental Information

Dual engagement of the NLRP3 and AIM2 inflammasomes by plasmodial-derived hemozoin and DNA during malaria

Parisa Kalantari[1], Rosane B. DeOliveira[1&], Jennie Chan[1&], Yolanda Corbett[2], Vijay Rathinam[1], Andrea Stutz[3], Eicke Latz[1,3], Ricardo T. Gazzinelli[1,4] , Douglas T. Golenbock[1*]and Katherine A. Fitzgerald[1*]

[1]Division of Infectious Diseases and Immunology, University of Massachusetts Medical School, Worcester, MA, USA 01605; [2]Dipartimento di Scienze Farmacologiche e Biomolecolari Universita Degli Studi di Milano, Via Pascal 36, Milano 20133, Italy; [3] Institute of Innate Immunity, Biomedical Center, 1G008, University Hospitals, University of Bonn, Sigmund-Freud-Str. 25, Bonn 53127, Germany [4]Department of Parasitology and Department of Biochemistry and Immunology, Biological Sciences Institute, Federal University of Minas Gerais, Av. Antonio Carlos 6627, Belo Horizonte, MG 31270, Brazil.

Fig. S1

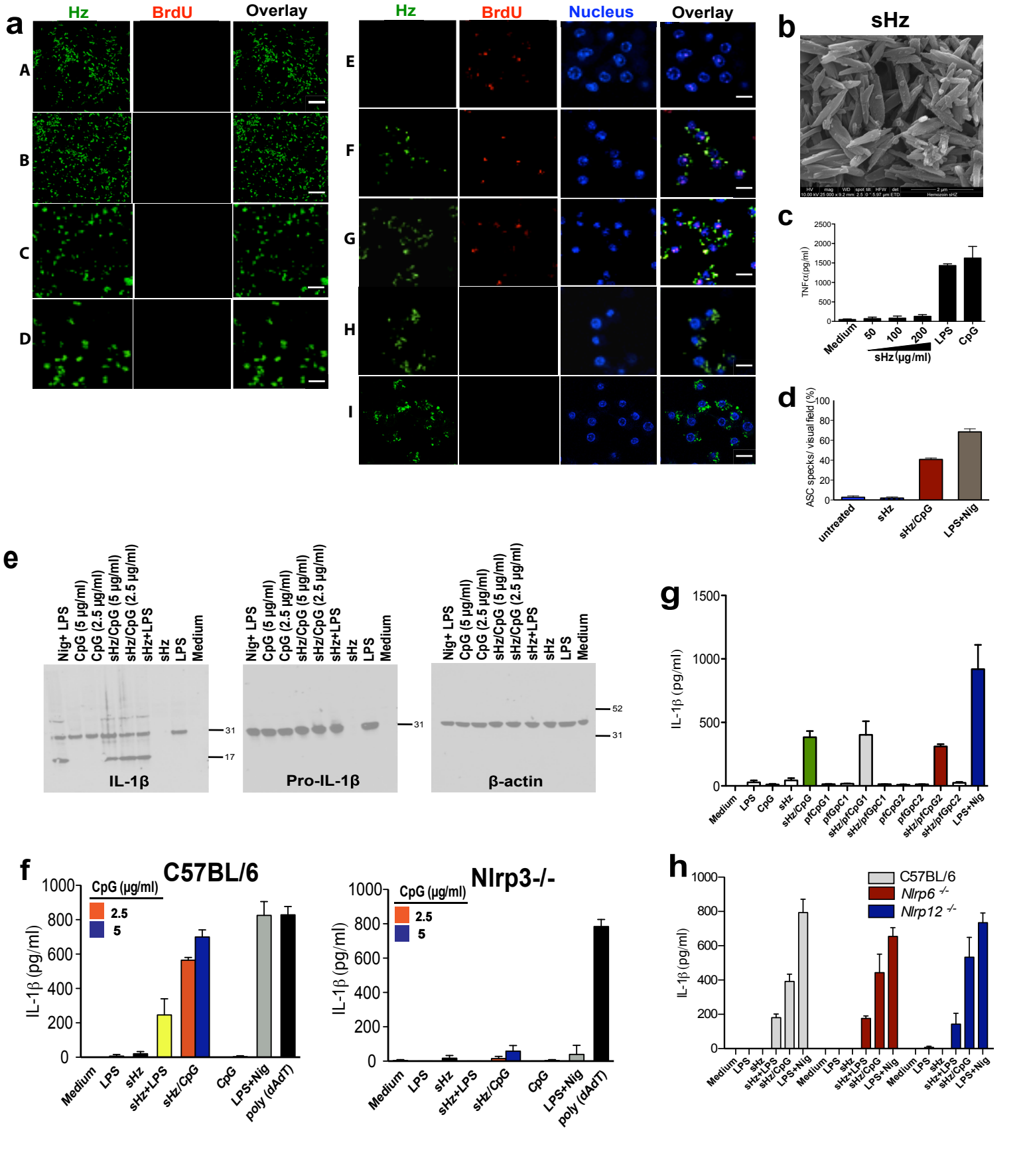
a
Hz
BrdU
Overlay
Nucleus
A
B
C
D
E
F
G
H
I
b
sHz
c
TNFα(pg/ml)
Medium
50
100
200
LPS
CpG
sHz (μg/ml)
d
ASC specks/ visual field (%)
untreated
sHz
sHz/CpG
LPS+Nig
e
Nig+ LPS
CpG (5 μg/ml)
CpG (2.5 μg/ml)
sHz/CpG (5 μg/ml)
sHz/CpG (2.5 μg/ml)
sHz+LPS
sHz
LPS
Medium
IL-1β
Pro-IL-1β
β-actin
31
17
52
g
IL-1β (pg/ml)
CpG
sHz
sHz/CpG
pfCpG1
pfGpC1
sHz/pfCpG1
sHz/pfGpC1
pfCpG2
pfGpC2
sHz/pfCpG2
sHz/pfGpC2
LPS+Nig
f
C57BL/6
Nlrp3-/-
CpG (μg/ml)
2.5
5
poly (dAdT)
h
C57BL/6
Nlrp6 -/-
Nlrp12 -/-

Figure S1 (Related to Figure 1): (a) **BrdU does not bind to synthetic and natural Hz.** Synthetic Hz was incubated with BrdU (A) and PBS (B) and nHz was incubated with BrdU (C) and PBS (D) for 2h at 37^{o}C. Synthetic Hz and nHz in A, B, C and D were washed with PBS X 3. Immortalized BMDMs were incubated with BrdU for 2h at 37^{o}C (E). Immortalized BMDMs were incubated with sHz for 6h and then treated with BrdU for 2h at 37^{o}C (F) Immortalized BMDMs were incubated with nHz for 6h and then treated with BrdU for 2h at 37^{o}C (G) Natural Hz was incubated with BrdU for 2h at 37^{o}C, washed 3 times with PBS and then incubated immortalized BMDMs with nHz for 6h (H) Synthetic Hz was incubated with BrdU for 2h at 37^{o}C, washed 3 times with PBS and then incubated immortalized BMDMs with nHz for 6h (I). BrdU concentration used in A-I was 10mM. DAPI and anti-BrdU mAb were used in Figures A-I as described in Materials and Methods and Hz was visualized using *reflection microscopy*. (b) **Scanning electron micrographs of sHz**. Sample was coated with Au/Pd of about 4 A^{o} in thickness and SEM pictures were taken using a FEI Quanta 200 MK II FESEM **(**c) **sHz is devoid of *Pf* gDNA and fails to elicit TNFα production.** Immortalized murine BMDMs were stimulated with different concentrations of sHz, CpG B (2.5μM), or 100ng/ml LPS for 12 h, and the production of TNFα was assessed by ELISA**.** (d) **sHz/CpG induces ASC pyroptososme formation in the absence of alternative priming signals.** Immortalized murine BMDMs stably expressing ASC-CFP were treated with sHz/CpG (5μg/ml), sHz only (100μg/ml) or LPS (100ng/ml) primed for 2h and then treated with nigericin (10μM). The formation of ASC pyroptosomes were quantified using confocal microscopy. Fields are representative of at least 10 fields of view and three independent experiments. (e) Original scans related to the composite blot shown in Fig. 1f **(**f**) sHz/CpG activates the NLRP3 inflammasome in primary macrophages without the**

need for alternative priming signals. ELISA of IL-1β production by primary C57BL/6 BMDMs and primary *Nlrp3*$^{-/-}$ BMDMs primed for with LPS (100ng/ml x 2h) and then left unstimulated or stimulated with sHz crystals (100μg/ml) or stimulated with sHz/CpG (5μg/ml), CpG (5μg/ml), nigericin (10μM), or poly(dAdT) (1.5. μg/ml). Supernatants were analyzed for IL-1β 12h after stimulation. (g) **sHz/*Pf* CpG complex mediates the release of mature IL-1β.** Immortalized murine BMDMs were stimulated with sHz coated with CpG 1826, *Pf*CpG1, *Pf*GpC1, *Pf*CpG2 or *Pf*GpC2 (sHz: 100μg/ml and CpG or GpC: 5μg/ml) and assayed by ELISA for released IL-1β. Sequences of the *Pf*CpG1, *Pf*GpC1, *Pf*CpG2 and *Pf*GpC2 are described in Ref (Parroche et al., 2007). (h) **sHz/CpG mediated release of IL-1β is NLRP6 and NLRP12 independent**. *Nlrp6*$^{-/-}$ or *Nlrp12*$^{-/-}$ primary macrophages were primed with LPS, or left untreated, and then stimulated with sHz crystals (100μg/ml) or sHz/CpG (5μg/ml) or nigericin (10μM). Supernatants were assessed for released IL-1β 12 hours later. Data are presented as mean of triplicate determinations ± SD and are representative of 3 independent experiments.

Figure S2

a

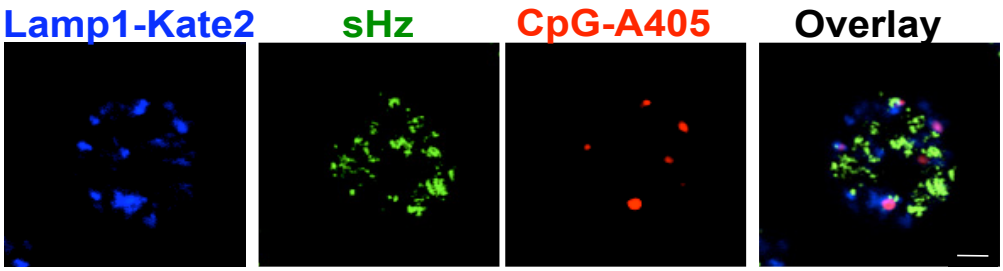
Lamp1-Kate2
sHz
CpG-A405
Overlay

b

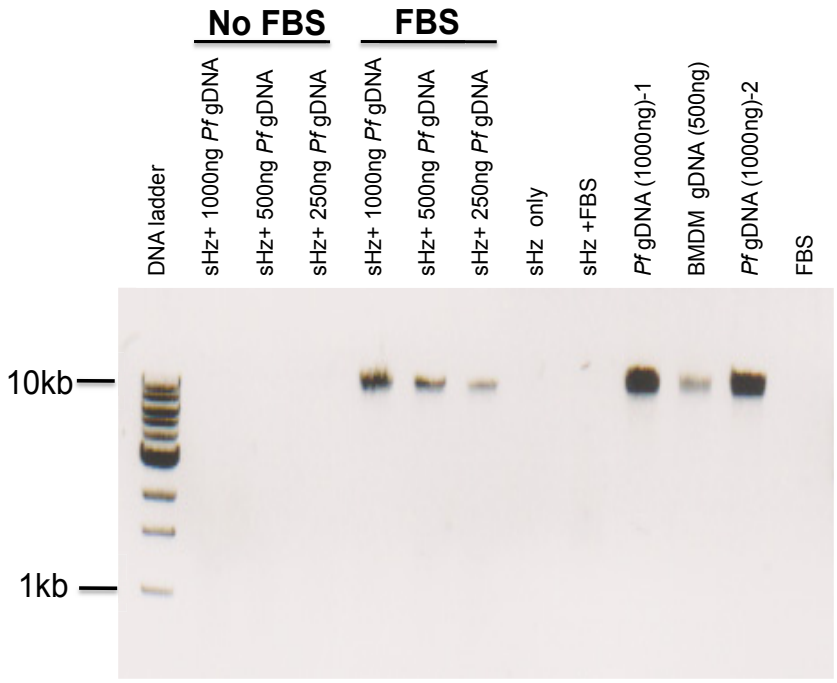
No FBS
FBS
DNA ladder
sHz+ 1000ng Pf gDNA
sHz+ 500ng Pf gDNA
sHz+ 250ng Pf gDNA
sHz+ 1000ng Pf gDNA
sHz+ 500ng Pf gDNA
sHz+ 250ng Pf gDNA
sHz only
sHz +FBS
Pf gDNA (1000ng)-1
BMDM gDNA (500ng)
Pf gDNA (1000ng)-2
FBS
10kb
1kb

Figure S2 (Related to Figure 2): (a) **sHz is released into cytosol while CpG remains bound to the phagosomal remnants of wt macrophages. Related to Figure 2.** (a) Confocal microscopy of immortalized murine BMDMs stably transduced with Lamp1-kate2, incubated for 6h with sHz/CpG (5μg/ml). Most sHz is released into cytosol, while CpG DNA stays in lysosomes. sHz was visualized using reflection microscopy (green). Scale bar: 5μm. Fields are representative of at least 10 fields of view and three independent experiments. (b) **Synthetic Hz coated with FBS binds to *Pf* gDNA.** 100 μg of sHz was left untreated or was coated with FBS overnight and then incubated with different amounts of *Pf* gDNA for 2h and washed 3x with PBS or incubated with gDNA (without coating with FBS) and washed 3x with PBS. The samples were run in a 1% agarose gel. As positive controls, 1000ng of *Pf* gDNA (1 and 2 are *Pf* gDNA extracted from malaria cultures at different times) and 500ng of immortalized murine BMDMs gDNA was used.

Figure S3

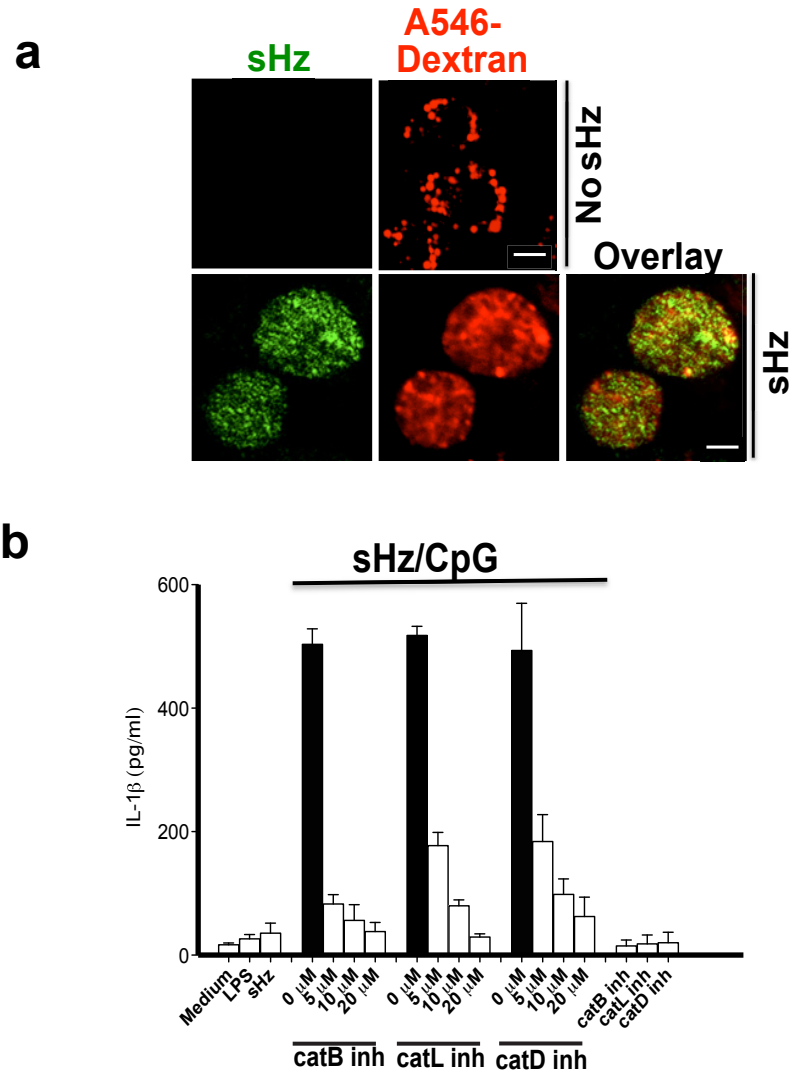
a
sHz
A546-Dextran
No sHz
Overlay
sHz
b
sHz/CpG
600
400
200
0
IL-1β (pg/ml)
Medium
LPS
sHz
0 μM
5 μM
10 μM
20 μM
0 μM
5 μM
10 μM
20 μM
0 μM
5 μM
10 μM
20 μM
catB inh
catL inh
catD inh
catB inh
catL inh
catD inh

Figure S3 (Related to Figure 3): (a) **Synthetic Hz induces phagolysosomal destabilization.** Confocal microscopy of immortalized murine BMDMs incubated with A546-Dextran 10kDa for 45 min and then either left untreated or stimulated with 100μg/ml sHz for 4 h. Reflection microscopy was used to visualize sHz (green). Scale bar (top and bottom panels: 10μm). The fields are representative of at least 10 fields of view and three independent experiments. (b) **Cathepsins are involved in sHz-mediated release of IL-1β.** Effect of various concentrations (0μM, 5μM, 10μM and 20 μM) of inhibitors of cathepsin B (catB inh), cathepsin L (catL inh) and cathepsin D (catD inh) on the sHz/CpG (5μg/ml) mediated release of IL-1β from wt murine immortalized BMDMs. Data are presented as mean ± SD of triplicates and are representative of 3 independent experiments.

Figure S4

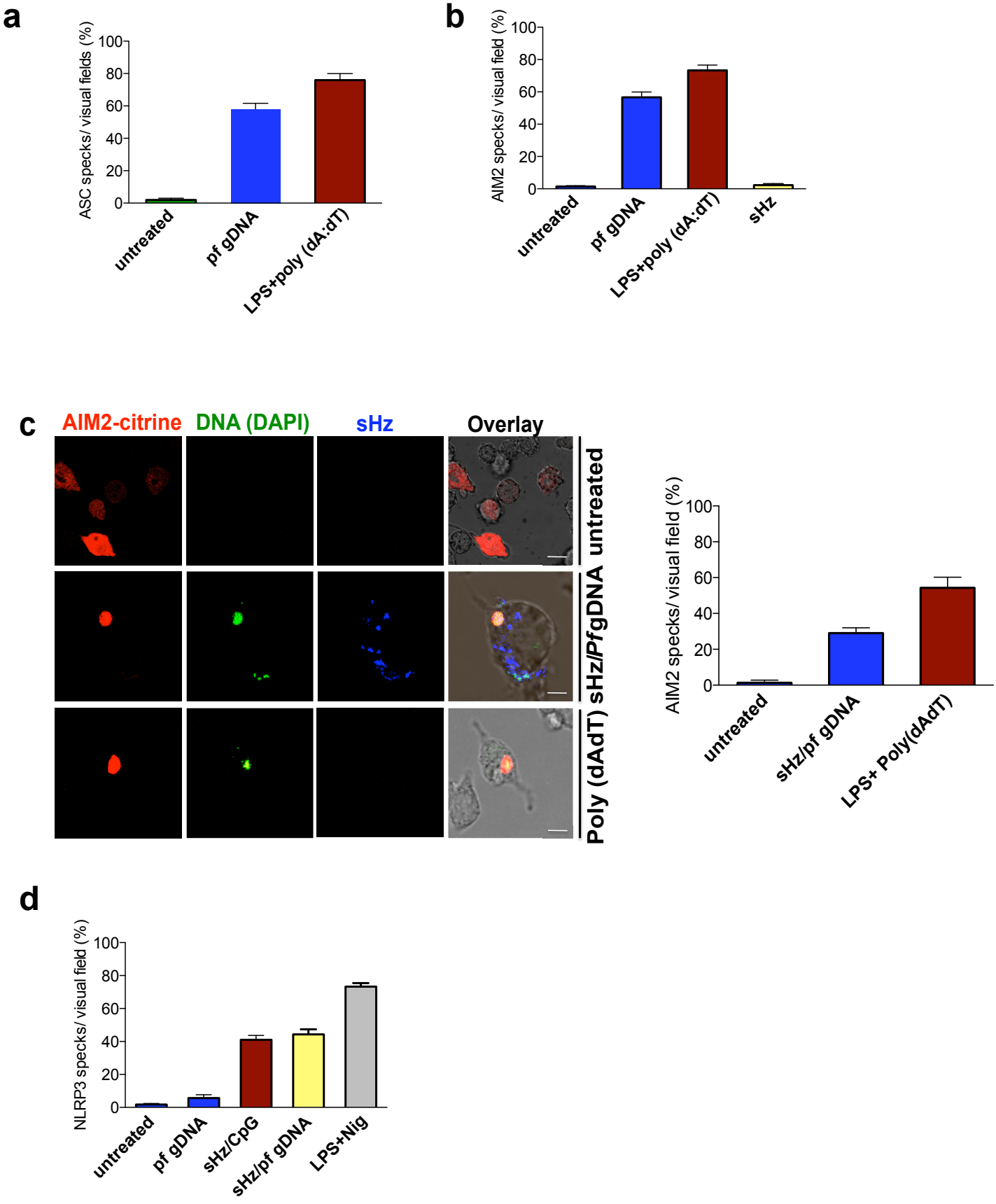
a
ASC specks/ visual fields (%)
100
80
60
40
20
0
untreated
pf gDNA
LPS+poly (dA:dT)
b
AIM2 specks/ visual field (%)
100
80
60
40
20
0
untreated
pf gDNA
LPS+poly (dA:dT)
sHz
c
AIM2-citrine
DNA (DAPI)
sHz
Overlay
untreated
sHz/PfgDNA
Poly (dAdT)
AIM2 specks/ visual field (%)
100
80
60
40
20
0
untreated
sHz/pf gDNA
LPS+ Poly(dAdT)
d
NLRP3 specks/ visual field (%)
100
80
60
40
20
0
untreated
pf gDNA
sHz/CpG
sHz/pf gDNA
LPS+Nig

Figure S4 (Related to Figure 4): (a) **Quantification of ASC and AIM2 speck formation in response to transfection of *Pf* gDNA.** Confocal microscopy of ASC-CFP stably expressing macrophages left untransfected or transfected with 100ng/ml Syto60-labeled *Pf* gDNA or Syto60-labeled poly (dAdT) using lipofectamine. The formation of pyroptosomes was quantified in 10-15 fields of cells by confocal microscopy. (b) AIM2-citrine stably expressing macrophages were left untransfected or LPS primed (2h, 100ng/ml) and then transfected with 100ng/ml DAPI-labeled *Pf* gDNA and DAPI-labeled poly (dAdT) using lipofectamine or sHz only (100μg/ml). The formation of AIM2 pyroptosomes was quantified using confocal microscopy (c) **The complex sHz/*Pf* gDNA induce AIM2 pyroptosome formation**. left panel: AIM2-citrine stably expressing macrophages were left untransfected or LPS primed (2h, 100ng/ml) and then transfected with DAPI-labeled poly (dAdT) using lipofectamine or incubated with DAPI-labeled sHz/*Pf*gDNA (4μg/ml). Scale bar: 20μm (top panel), 15μm (middle panel) and 25μm (bottom panel). Right panel: The formation of AIM2 pyroptosomes in figure shown in left panel was quantified using confocal microscopy (d) NLRP3-citrine stably expressing macrophages were left untreated or treated with sHz/CpG (5μg/ml), sHz/*Pf* gDNA (4μg/ml), nigericin or transfected with 100ng/ml *Pf* gDNA using lipofectamine. The formation of NLRP3 pyroptosomes was quantified using confocal microscopy. The fields are representative of at least 10 fields of view and three independent experiments.

Figure S5

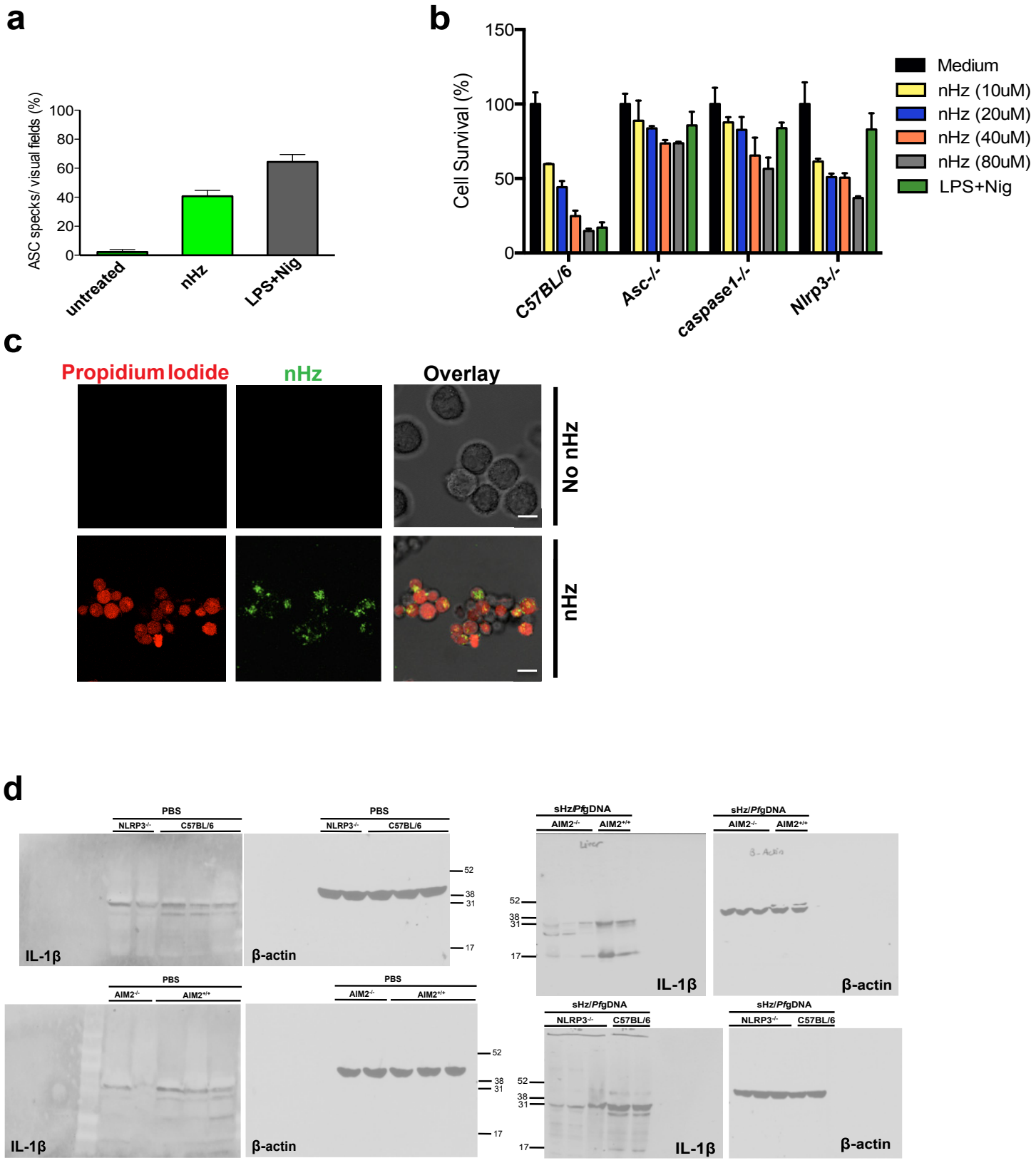
a
ASC specks/ visual fields (%)
100
80
60
40
20
0
untreated
nHz
LPS+Nig
b
Cell Survival (%)
150
100
50
0
C57BL/6
Asc-/-
caspase1-/-
Nlrp3-/-
Medium
nHz (10uM)
nHz (20uM)
nHz (40uM)
nHz (80uM)
LPS+Nig
c
Propidium Iodide
nHz
Overlay
No nHz
nHz
d
PBS
NLRP3-/-
C57BL/6
IL-1β
β-actin
52
38
31
17
AIM2-/-
AIM2+/+
sHz/PfgDNA

Figure S5 (Related to Figure 5): (a) **Quantification of ASC speck formation in response to nHz treatment.** ASC-CFP stably expressing macrophages were left untreated or treated with nHz (100μM). The formation of ASC pyroptosomes was quantified in 10-15 fields of cells by using confocal microscopy. (b) **nHz induced cell death is ASC, caspase-1 and NLRP3 dependent.** wt, *Asc*$^{-/-}$, *casp1*$^{-/-}$ and *Nlrp3*$^{-/-}$ immortalized murine BMDMs were incubated with 10 μM, 20 μM, 40μM and 80 μM of nHz for 12 h. Cell survival was measured using Calcein AM. Medium was set as 100%. Data are presented as mean ± SD of triplicates and are representative of 3 independent experiments. (c) wt BMDMs were incubated with 40μM nHz for 24h, then rinsed with PBS and stained with fluorescent Propidium Iodide. nHz was visualized using reflection microscopy (green). Scale bar: 30μm (top panel) and 20μm (bottom panel). Fields are representative of at least 10 fields of view and three independent experiments (d) Original scans related to the blot shown in Fig. 5d.

Figure S6

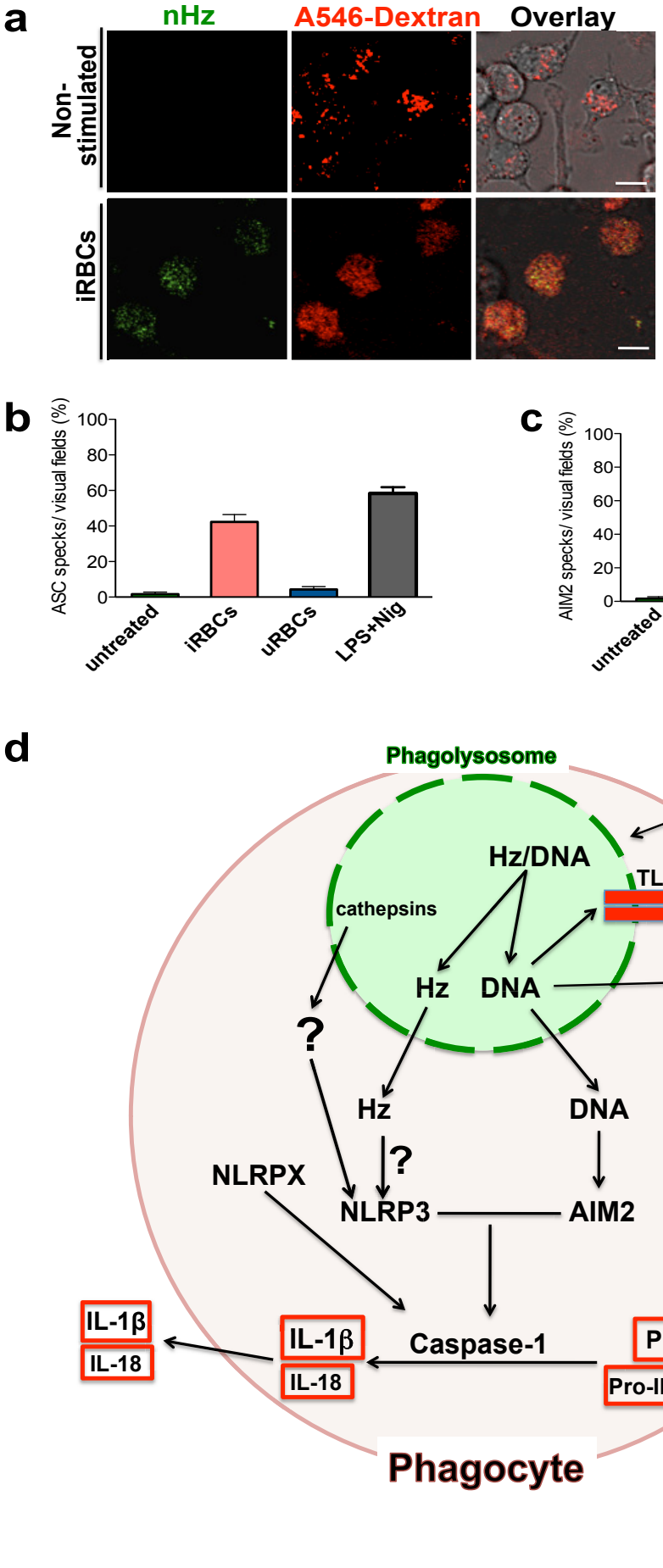
a
nHz
A546-Dextran
Overlay
Non-stimulated
iRBCs
b
ASC specks/ visual fields (%)
100
80
60
40
20
0
untreated
iRBCs
uRBCs
LPS+Nig
c
AIM2 specks/ visual fields (%)
100
80
60
40
20
0
untreated
iRBCs
uRBCs
LPS+poly (dA:dT)
d
Phagolysosome
Free Hz/DNA
Hz/DNA
TLR9
cathepsins
Hz
DNA
Type I IFNs
Ringed form
Schizont
?
Hz
DNA
?
NLRPX
NLRP3
AIM2
IL-1β
IL-18
IL-1β
IL-18
Caspase-1
Pro-IL-1β
Pro-IL-18
Phagocyte

Figure S6 (Related to Figure 6 and summary figure): (a) ***P. berghei*-RBCs induce phagolysosomal destablilization.** Confocal microscopy of immortalized BMDMs incubated with A546-Dextran 10kDa for 45 min and then either left untreated or stimulated with 8x 10^5 *P. berghei*-RBCs (iRBCs) for 18h. Reflection microscopy was used to visualize Hz. Scale bar (top and bottom panels: 15μm) (b) **Infected RBCs induce ASC and AIM2 speck formation.** ASC-CFP stably expressing macrophages were incubated with 8x 10^5 *P. berghei*-RBCs (iRBCs) or uRBCs for 12h and the formation of ASC pyroptosomes were quantified using confocal microscopy. (c) *P. berghei*-RBCs and uRBCs were incubated with DAPI for 1h and then co-cultured with AIM2-citrine macrophages for 12h. The formation of AIM2 pyroptosomes was quantified using confocal microscopy. Fields are representative of 10 fields of view and three independent experiments. (d) **Summary model of how Hz/DNA drives the innate immune response.** During the asexual phase of parasite life cycle, circulating schizonts release merozoites into the systemic circulation, as are fragments of parasites that are turning over within erythrocytes. Infected RBCs of all types (schizonts and ringed trophozoites are shown), as well as the liberated Hz that has been coated within the erythrocyte with DNA, encounter phagocytes. These microbial products, as well as iRBCs are internalized by phagocytosis. DNA on the surface of the Hz triggers TLR9 translocation and activation, which induces the transcriptional induction of NLRP3, pro-IL-1β and other NF-κB inducible genes, thus providing signal 1 for inflammasome activation. Once internalized, phagosomal enzymes digest the DNA off of the surface of the Hz. Hemozoin crystals subsequently destabilize the phagolysosome, providing access to the cytosol by the contents of this subcellular compartment. Hemozoin and *Plasmodium* gDNA are then released into the cytosol where they activate the NLRP3 and AIM2 inflammasomes. Cathepsins seem to be critical in Hz mediated inflammasome activation. It is not yet known if other inflammasomes ("NLRPX") play a role in IL-1β production, but this is likely. *Plasmodium* gDNA in the cytosol also triggers type I Interferon production. Activation of NLRP3 and AIM2 inflammasomes

(signal 2) leads to pro-IL-1β and pro-IL-18 cleavage and release of mature IL-1β and IL-18. The arrow shows the Hz crystal inside a *Pf* infected RBC (schizont).